Exploring the oxygen and carbon isotopic composition of the Mediterranean red coral (*Corallium rubrum)* for seawater temperature reconstruction

Chaabane, S.[*1, 2], López Correa, M.[3, 4], Montagna, P.[5], Kallel, N.[1], Taviani, M.[5, 6], Linares, C.[7], Ziveri, P.[2, 8]

1) University of Sfax, Lab. GEOGLOB, Route de Soukra, BP 802, 3038 Sfax, Tunisia.
2) Institute of Environmental Science and Technology (ICTA), Universitat Autonoma de Barcelona (UAB), 08193 Bellaterra, Barcelona, Spain.
3) GZN, GeoZentrum Nordbayern, Universität Erlangen-Nürnberg, Loewenichstr. 28, D-91054 Erlangen, Germany.
4) German University of Technology in Oman (GUtech), Department of Applied Geosciences, P.O. Box 1816, PC 130, Muscat, Sultanate of Oman.
5) ISMAR- CNR, Via Gobetti 101, 40129 Bologna, Italy.
6) Biology Department, Woods Hole Oceanographic Institute, 266 Woods Hole Road, MA 02543, USA.
7) Universitat de Barcelona, Departament d'Ecologia, 643 Diagonal Av., E-08028 Barcelona, Spain.
8) ICREA, Catalan Institution for Research and Advanced Studies, 08010 Barcelona, Spain

* *Corresponding author:* Sonia Chaabane (sonia.chaabane@gmail.com)

Abstract

Here we provide first evidence that the stable oxygen and carbon isotopic composition ($\delta^{18}O$, $\delta^{13}C$) of the high-magnesium calcite skeleton red coral *Corallium rubrum* can be used as a reliable seawater temperature proxy. This is based upon the analyses of living colonies of *C. rubrum* from different depths and localities in the Western Mediterranean Sea. The assessment of the growth rates has been established through the analysis of growth band patterns. The $\delta^{18}O$ and $\delta^{13}C$ compositions show large variability with a significant difference between the branches and the bases of the colonies. In both coral portions, the $\delta^{18}O$ and $\delta^{13}C$ values are highly correlated and show well-defined linear trends. Following the "lines technique" approach developed by Smith et al. (2000) for scleractinian aragonitic deep-water corals, our data have been combined with published values for the deep-sea gorgonian corals Isididae and Coralliidae from Kimball et al. (2014) and Hill et al. (2011) resulting in the following $\delta^{18}O$ temperature equation:

$$T\ (°C) = -5.05 \pm 0.24 \times (\delta^{18}O_{intercept}) + 14.26 \pm 0.43$$
$$(R^2 = 0.962,\ p\ value < 0.0001)$$

The error associated with this equation is ± 0.5 °C at the mean temperature of the data set, ± 0.7 °C for corals living in 2 °C water and ± 1 °C for coral living in warmer water (17 °C).

The highly significant $\delta^{18}O_{intercept}$ vs. temperature relationship combined with the "lines technique" method can be reliably applied to the calcitic skeleton to obtain calcification temperature estimates in the past, although this approach requires the knowledge of the past $\delta^{18}O$ and $\delta^{13}C$ composition of seawater and it is labor and time intensive.

Keywords

Red coral, Mediterranean Sea, Growth rings, $\delta^{18}O$, $\delta^{13}C$, Seawater temperature.

1. Introduction

Corals represent a valuable archive of paleoenvironmental conditions due to their wide spatial and vertical distribution in the global ocean. Specifically, several studies have proven that skeletal aragonite and calcite of scleractinian and gorgonian corals encode a rich record of ambient environmental conditions during skeletal formation, providing a key tool for paleoceanographic reconstructions (Adkins et al., 2003; Kimball et al., 2014; Montagna et al., 2007; Roark et al., 2005; Robinson et al., 2014; Sherwood and Edinger, 2009; Sherwood et al., 2008, 2005; Smith et al., 2000; Thresher et al., 2009, 2004; Tracey et al., 2007).

Much information is currently available on the geochemical response to climatic changes in the aragonitic skeletons of shallow and deep-water scleractinian corals (Gagan et al., 2000; McCulloch et al., 1999; Mitsuguchi et al., 1996; Montagna et al., 2005, 2006; Pelejero et al., 2005), while fewer comparable studies exist for calcitic corals, as for example for the bamboo corals *Keratoisis* (Hill et al., 2012, 2011; Sinclair et al., 2011; Thresher et al., 2009; Yoshimura et al., 2015) and the deep-sea coral specimens of the families Isididae and Coralliidae (Kimball et al., 2014).

Stable oxygen isotopes of marine biogenic carbonates have been widely used to reconstruct past ocean temperatures, since the pioneering study of Epstein et al. (1953) on mollusk shells. However, as already observed in other marine calcifying organisms (e.g. Bemis et al., 1998; Ziveri et al., 2012, 2003) $\delta^{18}O$ values in scleractinian corals, especially in deep-water corals, often differ from the expected thermodynamic equilibrium values due to "vital effects" (Adkins et al., 2003; McConnaughey, 1989). For the majority of the tropical corals studied so far, the quasi-constant $\delta^{18}O$ disequilibrium offset enables the application of species-specific and site-specific calibration equations (Gagan et al., 1994; Leder et al., 1996), which take into account and correct for the "vital effects" on $\delta^{18}O$. On the other hand, this empirical approach seems unattainable for deep-water corals that show a much wider range of $\delta^{18}O$ and $\delta^{13}C$ within their skeleton (indicative of strong "vital effects") (Adkins et al., 2003; López Correa et al., 2010) and do not exhibit evident seasonal growth bands like their tropical counterparts. However, based on the fact that some skeletal portions of deep-water corals approach isotopic equilibrium for $\delta^{18}O$ and $\delta^{13}C$, Smith et al. (2000) developed a method to obtain paleotemperatures from scleractinian deep-water corals. This so called "lines technique" approach consists of calculating a linear regression between the ambient temperatures and the equilibrium $\delta^{18}O$ values, which are identified as the value of the coral at $\delta^{13}C_{coral}$ = ambient $\delta^{13}C_{DIC}$ (DIC = Dissolved Inorganic Carbon) along a regression line of multiple $\delta^{18}O$ vs. $\delta^{13}C$ values within the skeleton of an individual coral. This method has been recently applied also to calcitic Isididae and Coralliidae corals spanning a range of temperatures from 2.0 to 11.2 °C (Hill et al., 2011; Kimball et al., 2014). A general temperature vs. $\delta^{18}O_{intercept}$ equation for calcitic corals has been calculated (Kimball et al., 2014) with a best-estimated precision of ±0.5 °C.

The family Coralliidae has a fossil record dating back at least to the Miocene (Vertino et al., 2010). At present the family includes some 20 species distributed in all oceans, generally at depths greater than 500 m (Bayer and Cairns, 2003), with the noticeable exception of *Corallium rubrum*, which is preferentially distributed at shallower subtidal depths. *Corallium rubrum* (Linnaeus, 1758) is a gonochoric slow-growing gorgonian coral (Anthozoa, Gorgonacea) that thrives in subtidal to bathyal habitats in the Mediterranean Sea and the Eastern Atlantic Ocean (Cattaneo-Vietti and Cicogna, 1993; Chintiroglou et al., 1989; Rossi et al., 2008; Taviani et al., 2011; Zibrowius et al., 1984). This species has been commercially harvested since ancient times for the high economic value of its red axial calcitic skeleton (Taviani, 1997; Tescione, 1973; Tsounis et al., 2007).

In this paper, four living specimens of the Mediterranean red coral *Corallium rubrum* were collected from different sea floor environmental conditions and studied with focus on their growth band pattern and stable isotopic compositions ($\delta^{18}O$ and $\delta^{13}C$). We applied the "lines technique" method of Smith et al. (2000) to the skeleton of *C. rubrum* extending the calibration for calcitic corals over a temperature range from 2°C to 17°C. The aim of the study was to test the ability of this coral species to serve as a reliable archive of seawater temperature.

2. Materials and methods

2.1. Coral sampling

Four living specimens of *C. rubrum* were collected by SCUBA diving in the Western Mediterranean Sea at different depths and from different environmental settings (Figure 1, Table 1), to explore the effect of seawater temperature on their $\delta^{18}O$ and $\delta^{13}C$ values. In particular, three small colonies were retrieved from Riou Island near Marseille, Medes Islands (Spain) and Scandola (Corsica) in June and July 2008 at 15 m, 18 m and 21 m, respectively. The fourth colony was collected off Portofino (Italy) in May 2009 at deeper depth (50 m). (Table 1, Figure1).

2.2. Environmental settings

Hourly seawater temperature series were obtained from the T-MedNet network (www.t-mednet.org). This network has acquired temperature data in Corsica and Medes Islands since 2004 and in Riou Island since 2003 using autonomous temperature data loggers (StowAway TidibiT). The annual mean temperatures at the shallowest Mediterranean North western sites in Riou Island, Medes Islands and Corsica are similar (16.37, 16.45 and 17.34°C respectively) (Table 1) whereas it is lower nearby Portofino (14.61°C), obtained from the NOAA NODC WOA13 database (Boyer et al., 2013). The seasonal temperature variability differs strongly between the different sites (Fig. 2). The largest variability is evidently encountered at the shallowest sites with 6.70°C at Riou Island, 8.52°C at Corsica, and 8.62°C at Medes Islands. At 50 m off Portofino the seasonal variability is reduced to ~ 3.95°C. The temperature range for the Medes Islands, Riou Island and Corsica has been calculated from the high resolution temperature data acquired from T-MedNet network.

The sites of Riou Island, Medes Islands and Corsica are predominantly influenced by the Northern currents, the Northwestern and Northern orographic winds (Tramontana and Mistral) promoting deep and cold water upwelling, and the Rhône river fresh water input, whose plume can extend to the Spanish coast to the West and to the Marseilles Gulf to the East (Bavestrello et al., 1993; Bensoussan et al., 2010; Linares et al., 2013; Millot, 1990, 1979; Petrenko, 2003; Salat and Pascual, 2002; Vielzeuf et al., 2013; Younes et al., 2003). In addition, in the Medes Islands some episodes of surface T inversion during winter can also be caused by the influence of the Ter River, located 5 km south of the islands (Salat and Pascual, 2002. Bensoussan et al., (2010) showed that the summer temperature in the Medes Islands is around 22-24°C close to the water surface and around 18-20°C at depth (40 m); whereas in Riou Island repetitive deep and cold upwelled waters have been noted due to the strong influence of the Rhône River and mistral winds. The water column stratification in Corsica is stable in summer (Bensoussan et al., 2010; www.t-mednet.org).

Despite the different locations and depth of the samples, the salinity values are similar with annual mean values ranging from 37.748 at Medes Islands to 38.015 at the site of Portofino (NOAA NODC WOA13 database) (Table 1).

The oxygen isotopic values of the ambient seawater were sourced from the NASA GISS LeGrande_Schmidt2006 v1p1 $\delta^{18}O$ (Grid-1x1) database (LeGrande and Schmidt, 2006) that covers wide areas and depths in the western Mediterranean. These values are reported relative to the Vienna Standard Mean Ocean Water (V-SMOW) and range from 1.31‰ to 1.39‰ V-SMOW which are comparable to that reported in Pierre (1999) (between 0.76‰ and 1.37‰ V-SMOW in the surface). Seawater $\delta^{13}C$ ($\delta^{13}C_{DIC}$) values were selected from Pierre (1999) and are reported relative to Vienna Pee Dee Belemnite (V-PDB). In the Western Mediterranean they vary between 0.87‰ and 1.50‰ V-PDB (Pierre, 1999) and strongly depend on the CO_2 exchange between the atmosphere and the surface water as well as on exchange with deep water. The $\delta^{13}C$ values around the Riou Island are lower compared to the other studied sites due to the injection of old CO_2 from intermediate and deep waters to the surface during winter mixing (Pierre, 1999).

Ambient seawater $\delta^{18}O$ compositions and temperatures were used to calculate the expected calcite $\delta^{18}O$ values based on the inorganically-precipitated calcite equation of Kim and O'Neil (1997) for low-temperature (10-40 °C), which was modified by Bemis et al. (1998) using a quadratic approximation.

2.3 Sample preparation

2.3.1 Thin section

The coral specimens were first photographed for documentation and then cut with a diamond blade above the colony base and perpendicular to the growth direction of the stem. Stem and branch sections of the samples from Portofino, Medes Islands and Riou Island were embedded in epoxy resin (Araldit and Araldur) and cured at room temperature for 24h. The epoxy blocs were cut and shaped with a Buehler ISOMET low-speed saw, polished in several steps with silicon carbide powder (800 grit) and glued to the glass slides. The sections were finally polished to a thickness of 70 - 35 µm and cleaned in an ultrasonic bath.

2.3.2 Organic matrix staining

Thin sections were treated following the organic matrix staining approach of Marschal et al. (2004). Briefly, the thin sections were decalcified in 2% acetic acid solution for 4 to 5 h, then gently rinsed in tap water and stained with Toluidine blue at 0.05% for 10–30 s and finally air-dried. Some thin sections were repeatedly stained to improve the visualization of the organic matrix rings under a stereomicroscope. After decalcification, special care was taken in the handling of the slabs to avoid breakage of the delicate organic matrix structure. These stained thin sections were observed under the stereomicroscope for growth ring counting.

2.4. Age determination

Estimates of the age of the colonies and their growth rate (in the annular zone) were based on counting the alternating dark and light blue growth rings in the etched and stained thin section observed under the stereomicroscope (Marschal et al., 2004) (Figure 3).

To minimize error in age determination, we deliberately avoided investigating the skeleton portion close to the oldest and youngest polyps of the colony, as well as the crowded and missing zone where the rings are very close, cut or stuck to each other. The rings were analyzed in different portions of the annular part of the axial skeleton of each specimen to improve the ring counting. The thicknesses of the growth rings were calculated using the publically accessible image-processing program Image J (Schneider et al., 2012).

2.5. Carbonate micro-sampling for $\delta^{18}O$ and $\delta^{13}C$

Micro-meter scale sampling of carbonate powders for stable isotope analyses was carried out along the entire stem diameter of the four specimens using a Merchantek

Micromill (New Wave) at GeoZentrum Nordbayern (GZN) in Germany. Individual transects measured ~2.5 mm in length, 50 µm in width and 150 µm in depth and were oriented parallel to the growth increments at intervals of about 90 µm for Portofino (PF), 93 µm for Medes Islands (MI), 83 µm for Riou Island (RI) and 80 µm for Corsica (CO) (Figure 4). Some of the micromill transects were defined following the growth layers that were visible without staining the organic matrix whereas other tracks were generated automatically by the computerized Micromill all the way through the coral skeleton surface (i.e. at constant spacing). The created tracks vary hence slightly per individual, but grant for the highest feasible spatial resolution.

2.6. Mass Spectrometry

Aliquots containing ~25 µg of coral material were analyzed for carbon and oxygen isotopes at GZN in Germany. Carbonate powders were reacted with 100% phosphoric acid at 70°C using a Gasbench II connected to a Thermo Delta V Plus isotope ratio mass-spectrometer. All values are reported in ‰ relative to Vienna Pee Dee Belemnite (V-PDB) by assigning a $\delta^{13}C$ value of +1.95‰ and a $\delta^{18}O$ value of -2.20‰ to NBS 19. The overall external analytical precision, based on 39 replicate analyses of the certified standard NBS 19, was better than ± 0.09 ‰ and ± 0.04 ‰ (1SD) for $\delta^{18}O$ and $\delta^{13}C$, respectively. The data are presented in the conventional delta-notation:

$$\delta^{18}O_{sample} = ((^{18}O/^{16}O)_{sample} / (^{18}O/^{16}O)_{standard}) - 1) \times 1000$$

3. Results

3.1 Age and growth rates

Based on the organic matrix staining method of Marschal et al. (2004), the estimated coral ages in the Medes Islands, Portofino and Riou Island sites are 30 ± 1, 27 ± 6 and 18 ± 2 years, respectively (Table 2). In the cross-sections, coral growth bands are partly intersected or discontinuous especially close to the area of the medullar zone. This is particularly the case for the coral from the Portofino site leading to slightly distinct number of growth bands in the different compartments of the coral and thus higher age error. An insignificant correlation was found between the basal diameter and the number of growth rings (R = 0.533 and ρ = 0.642). This is probably due to the low number of analyzed specimens and their distinct sampling locations. The ring thickness within the annular zone varies along the growth direction, with the annual rings becoming narrower towards the external edge of the coral. Accordingly, the growth rate decreases as the age of the colony increases, from 85 ± 12 µm/yr for the youngest colony (Riou Island) to 56 ± 6 µm/yr for the oldest colony (Medes Islands) (Table 2). The sample from Portofino has an average growth rate of 118 ± 3 µm/yr. The mean growth rate calculated by dividing the basal diameter by the number of growth rings varies from 172 ± 7 µm/yr for the specimen from Medes Islands to 276 ± 65 µm/yr for the deeper sample from Portofino (Table 2).

3.2 Stable isotope variation

Tables 3 and 4 report the $\delta^{18}O$ and $\delta^{13}C$ values of the annular and medullar zones of the four specimens analyzed, the mean values (±1SD) and the isotopic range for the entire stem, annular and medullar portions. The $\delta^{18}O$ and $\delta^{13}C$ vary from -2.70 to 0.89‰ and -6.35 to -0.27‰, respectively, with the largest variations observed for the Portofino specimen. Overall, the coral branches show more negative $\delta^{18}O$ and $\delta^{13}C$ values compared to the bases (Tables 3, 4, Figs. 5 and 6). Furthermore, the $\delta^{18}O$ and $\delta^{13}C$ values exhibit large variations across the annular and medullar portions of the axial skeleton (Fig. 5). The medullar zone generally presents slightly more negative $\delta^{18}O$ and $\delta^{13}C$ values (from -2.70 to 0.83‰ and from -6.35 to -0.27‰, respectively) compared to the annular zone (from -1.04 to 0.89‰ for $\delta^{18}O$ and from -5.19 to -0.69‰ for $\delta^{13}C$), especially for the specimens from Portofino, Riou Island and Corsica (Figure 5A, 5C and 5D; Table 4). In particular, the larger annular vs. medullar variation is observed for the specimen collected off Portofino (Figure 5A). Here the difference in isotopic composition between the annular and medullar zone is 3.93‰ for $\delta^{13}C$ and 2.46‰ for $\delta^{18}O$. On the other hand, the sample from Corsica shows the smallest variation, with a maximum difference between the medullar and the annular portions of 1.43‰ for $\delta^{13}C$ and 0.88‰ for $\delta^{18}O$. This is mainly due to the fact that the sub-samples were collected mostly within the annular zone and close to the medullar zone. Figure 5B shows the variation of the $\delta^{18}O$ and $\delta^{13}C$ values across the skeleton base of the coral collected from Medes Islands. The $\delta^{13}C$ mean value for the annular zone (-1.94 ± 0.72 ‰) is similar to that in the medullar zone (-1.91 ± 0.32‰). However, the annular zone shows a higher $\delta^{13}C$ variation compared to the medullar zone. The mean $\delta^{18}O$ values are -0.03 ± 0.26‰ in the annular zone and -0.45 ± 0.27‰ in the medullar part.

The $\delta^{18}O$ values of the coral were compared to the expected equilibrium $\delta^{18}O$ values calculated using the equation by Bemis et al. (1998) (Table 4). All the coral values are consistently offset from the $\delta^{18}O$ equilibrium, showing the biological imprint on the $^{18}O/^{16}O$ fractionation during the skeleton formation (vital effect). In particular, the annular and medullar zones in the branch fragments from Riou Island and Corsica show $\delta^{18}O$ values that are lower by 1.43 ± 0.04‰ and 1.71 ± 0.02‰, respectively with respect to the expected equilibrium values (Table 4). A smaller $\delta^{18}O_{coral}$ - $\delta^{18}O_{equilibrium}$ difference is observed for the annular zone of the base of the colony from Medes Islands (1.01 ± 0.01‰), suggesting that calcite forming the basal stem of *C. rubrum* precipitates closer to equilibrium compared to the calcite of the branches (see discussion).

Similarly, the coral $\delta^{13}C$ values are more negative when compared to the expected equilibrium $\delta^{13}C$ calculated using the equation by Romanek et al. (1992) (Table 4), with the $\delta^{13}C$ composition of the basal stem being about 1‰ closer to equilibrium than the branches (i.e. 4.19 ± 0.36‰ for the basal portion and 5.84 ± 0.74‰ for the branches).

3.3 $\delta^{13}C$ vs. $\delta^{18}O$

The $\delta^{13}C$ vs. $\delta^{18}O$ results show highly significant linear regressions, both in the annular and medullar zone (R^2 between 0.33 and 0.70), but generally display different slopes for the different coral portions (Fig. 5, Table 5). Overall, the medullar zone shows a steeper $\delta^{13}C$ vs. $\delta^{18}O$ slope and higher intercept values compared to the annular portion (Fig. 5). A positive and highly significant $\delta^{13}C$ vs. $\delta^{18}O$ linear regression is also observed when considering all the data together ($R^2 = 0.62$, p value <0.0001) (Fig. 6).

Figure 7 shows the different $\delta^{13}C$ vs. $\delta^{18}O$ linear regressions in the analyzed coral portions (medullar vs. the two annular zones) for all the specimens investigated. With the exception of the sample from Corsica, for which all the regression slopes are very similar, the regressions between $\delta^{13}C$ and $\delta^{18}O$ values for the other specimens show distinct slopes and intercepts. Furthermore, the coefficients of determination decrease when the two annular zones are considered separately, in particular for the sample from Medes Island (Fig. 7B).

Despite these differences, the mean $\delta^{13}C$ and $\delta^{18}O$ values are generally the same, within error, across the two different sides of the annular zone (Table 6).

Following the "lines technique" approach, the $\delta^{18}O_{intercept}$ for each specimen was obtained from the least squares linear regression analysis of coral $\delta^{18}O$ vs. $\delta^{13}C$ (corrected for local $\delta^{18}O_{sw}$ and $\delta^{13}C_{DIC}$) at $\delta^{13}C = 0$‰. The calculated $\delta^{18}O_{intercept}$ values were finally plotted against the ambient seawater temperatures, together with published data from Hill et al. (2011) and Kimball et al. (2014), and a general linear regression was derived over a temperature range from 2°C to 17.34°C.

4. Discussion

4.1. Growth rate

Our findings on *C. rubrum* growth rates ranging from 172 ± 7 to 276 ± 65 µm/year are consistent with previous estimates provided by Bramanti et al., (2014) (0.241±0.061 and 0.237±0.062 mm/year for specimens from Portofino and Cap de Creus), Benedetti et al., (2016) (0.26±0.07 and 0.21±0.08 mm/year for specimens from the North and Central Tyrrhenian Sea), Vielzeuf et al., (2013) (0.200±0.02 mm/year for a specimen from Medes Islands) and Garrabou and Harmelin, (2002) (0.240±0.05 mm/year for corals from Riou Island).

The average annual growth rates, determined either by dividing the basal diameter by the number of growth rings or by selecting only the annular portion (Table 2), indicate a certain variability between the shallower and deeper coral specimens, with the sample from Portofino (50m water depth) growing twice as fast as the specimen from Medes Islands (18m water depth). This difference in growth rate is still significant even when the errors in age estimation are taken into account, suggesting a biological response of the coral to different site-related environmental conditions, such as for example a greater availability of resuspended detrital particulate organic matter in deeper zones, as reported by Tsounis et al., (2006). This could eventually provide more energy supply for the coral to increase its growth rate. On the other hand, the growth rate of *C. rubrum* decreases at high temperatures (Vielzeuf et al., 2013) and this could explain the lower value for the samples from Medes Islands and Riou Island compared to the one from Portofino. However, the specimen from Riou Island is growing faster than the coral from Medes Islands even though the seawater temperature of the two sites is similar, likely suggesting a decrease in growth rate with colony age as observed by Bramanti et al. (2014). A detailed study should be conducted to identify the environmental factors controlling *C. rubrum calcification*, combining growth rate measurements of various specimens with critical seawater parameters (e.g. temperature, nutrient content, seawater carbonate chemistry, etc.).

4.2. *δ¹⁸O and δ¹³C composition of C. rubrum*

The strong linear regressions between $\delta^{18}O$ and $\delta^{13}C$ values obtained for the high Mg calcite (HMC) skeleton of *C. rubrum* specimens (Fig. 5) are consistent with the $\delta^{18}O$-$\delta^{13}C$ relationship often observed for aragonitic shallow and deep-water corals (e.g. Adkins et al., 2003; López Correa et al., 2010; McConnaughey, 1989) as well as for other calcitic corals (Hill et al., 2011; Kimball et al., 2014; Yoshimura et al., 2015). Moreover, similarly to scleractinians and other calcitic coral species, the oxygen and carbon isotopic composition of the Mediterranean *C. rubrum* is strongly depleted in ^{18}O and ^{13}C relative to inorganically-precipitated calcite (Table 4). This is especially the case for the medullar zone in the coral branches characterized by $\delta^{18}O$ and $\delta^{13}C$ values shifted by almost 2‰ from the expected equilibrium based on ambient seawater temperature. Both the annular and medullar zones for the basal portion and the branches display a large variation in $\delta^{18}O$ and $\delta^{13}C$ over short distances (Table 4) that cannot be explained by water temperature fluctuations. If the micro-meter variations in oxygen isotopes across the micromill transects are converted to seawater temperature using, for example, the equation by Bemis et al. (1998), the calculated range would be equivalent to more than 12°C for the Portofino specimen, which is much higher than the seasonal fluctuation recorded at the sampling location (Fig. 2). Moreover, considering that the micromill sampling resolution (80 to 93 μm intervals) integrated approximately one year, the calculated temperature range far exceeds the interannual variability. This clearly means that seawater temperature does not represent the major controlling factor of the variability in $\delta^{18}O$ values in ontogenetic transects of *C. rubrum*. Similar conclusions were drawn for the magnesium distribution in *C. rubrum* by Vielzeuf et al., (2013), which suggested a minor temperature control on magnesium incorporation. As extensively reported for other scleractinian and gorgonian coral species, the Mediterranean HMC coral *C. rubrum* seems also to exert a strong physiological control on the fractionation of stable isotopes and the uptake of trace elements. Biologically-induced isotopic fractionation shifts the $\delta^{13}C$ and $\delta^{18}O$ composition towards more negative values relative to expected equilibrium and generates large micro-meter scale isotopic variability that is not proportional to seawater temperature or seawater chemistry variations. As suggested for tropical and cold-water scleractinian corals, the observed deviation of the $\delta^{18}O$ values from expected equilibrium might be the result of the kinetic effects associated to the hydration and the hydroxylation reactions of the CO_2 during the coral skeleton formation (McConnaughey, 1989). In particular, the kinetic model assumes that skeleton precipitation occurs faster than the complete isotopic equilibration of HCO_3^- with H_2O, preventing the coral skeleton to reach oxygen isotopic equilibrium. This model would also explain the difference in $\delta^{18}O$ between the colony base and coral branches, with the latter growing faster and showing more negative $\delta^{18}O$ values compared to the coral base (Table 4).

Overall, our micromill isotope data clearly show that there is not a simple dependency of *C. rubrum* $\delta^{18}O$ with seawater calcification temperature. Conversely, following the "lines technique" approach by Smith et al. (2000) for scleractinians and recently applied to calcitic corals (Hill et al., 2011; Kimball et al., 2014), the strong relationship between the $\delta^{18}O$ and $\delta^{13}C$ values and their intercept may be a valuable proxy for ocean temperature.

4.3. C. rubrum as a temperature archive

The coral $\delta^{18}O$ values calculated from the linear regression equations $\delta^{18}O$ vs. $\delta^{13}C$ for the annular zone (corrected for local $\delta^{18}O_{sw}$ and $\delta^{13}C_{DIC}$) at $\delta^{13}C$ = 0‰ vary from -0.52 to 0.33 (Table 7). These $\delta^{18}O$ intercept values were compared with those calculated by Kimball et al., (2014) and Hill et al. (2011) (modified by Kimball et al., 2014) for the calcitic Isididae and Coralliidae corals spanning a range of temperatures from 2 to 11.2 °C (Fig. 8). Overall, the $\delta^{18}O_{intercept}$ values obtained from the *C. rubrum* specimens plot close to the confidence interval of the regression line calculated by Kimball et al. (2014) (Fig. 8), although they are slightly higher to what expected considering the ambient seawater temperature. The relatively poor fit between our data and the regression line of Kimball et al. (2014) extrapolated for higher temperatures is puzzling. It might be partially related to the seawater $\delta^{18}O$ and $\delta^{13}C$ values used to calculate the $\delta^{18}O$ intercepts for *C. rubrum*. In fact, this calculation is sensitive to the seawater isotopic values applied to correct coral $\delta^{18}O$ and $\delta^{13}C$; for example, the $\delta^{18}O_{intercept}$ value for the Medes Islands sample would change from -0.52 to -0.68 if using $\delta^{18}O_{sw}$ of 1.39‰ (instead of 1.31‰) and $\delta^{13}C_{DIC}$ of 0.87‰ (instead of 1.20‰). Similarly, some of the $\delta^{18}O_{intercept}$ values calculated by Kimball et al. (2004) using available seawater $\delta^{18}O$ and $\delta^{13}C$ sourced from database (e.g. WOCE) might be not entirely accurate. Other possible explanations for the relatively poor fit are laboratory offsets in $\delta^{18}O$ and $\delta^{13}C$ and potential species-specific fractionation of oxygen and carbon isotopes during the skeleton formation of calcitic corals (i.e. Isididae vs. Coralliidae). Although our data do not perfectly plot on the extrapolated regression line of Kimball et al. (2014), they are consistent with the general trend of decreasing $\delta^{18}O_{intercept}$ values with increasing temperature. Therefore, we decided to derive a general $\delta^{18}O_{intercept}$ vs. temperature equation by combining our data with those of Kimball et al. (2014) and Hill et al. (2011) (Fig. 8A):

$$T\,(°C) = -5.2 \pm 0.33 \times (\delta^{18}O_{intercept}) + 14.64 \pm 0.58 \qquad (1)$$

$$(R^2 = 0.937,\ p\text{-value} < 0.0001)$$

The $\delta^{18}O$ intercept values for *C. rubrum* slightly change when excluding a few very negative $\delta^{18}O$ and $\delta^{13}C$ data points in the annular zone of the coral branches of the Riou Island and Corsica samples (Fig. 5 and table 7). These “anomalous” points, with $\delta^{18}O$ and $\delta^{13}C$ values lower than the average minus the standard deviation of the annular zone, have values comparable to those measured in the medullar zone, suggesting a stronger biological control. These micro-meter scale portions within the annular zone are most likely the result of the irregular shape of the medullar portion (see Fig. 3) and the micromill transect intercepting multiple medullar sub-regions. By rejecting those values from the annular zone, the newly calculated $\delta^{18}O_{intercept}$ values for Riou Island and Corsica (-0.18 and -0.22, respectively; Table 7) approach the values obtained from the basal portions.

The $\delta^{18}O_{intercept}$ vs. temperature relationship using the new values together with the data by Kimball et al. (2014) and Hill et al. (2011) yields the following calibration equation (Fig. 8B):

$$T\,(°C) = -5.05 \pm 0.24 \times (\delta^{18}O_{intercept}) + 14.26 \pm 0.43 \qquad (2)$$

$$(R^2 = 0.962,\ p\text{-value} < 0.0001)$$

The overall precision is ± 1°C, as quantified by the standard error of estimates calculated from Bevington and Robinson, (1992). Compared to Kimball et al. (2014), this new equation improves the temperature estimates for calcitic corals living in warmer temperature. The errors in the temperature estimates were calculated based on the 95% confidence intervals and correspond to ± 0.5 °C for $\delta^{18}O_{intercept}$ values near the average of the data set (1.44‰), ± 0.7 °C for lower temperatures (2°C) and ± 1 °C for warmer temperatures (17°C).

Equations 1 and 2 are similar within error and present a maximum of ~ 0.5°C difference at highest temperature for a given $\delta^{18}O_{intercept}$. The $\delta^{18}O$ vs. temperature sensitivity for both regression lines is parallel to expected $\delta^{18}O$ equilibrium values based on the inorganically-precipitated calcite equation of Shackleton, (1974) and Kim and O'Neil (1997) modified by Bemis et al. (1998) (Fig. 8). Moreover, the slopes of the biologically-precipitated calcite equations (-5.2 and -5.05) also approximate the slope of the biogenic aragonite temperature equation (-4.34; Grossman and Ku, 1986) (Fig. 8). However, there is a clear shift in the intercept, which reflects the fact that an isotopic fractionation exists between aragonite and calcite (~ 0.8 ‰ at 25°C; Kim et al., 2007).

The consistency of our data for *C. rubrum* to those obtained from Hill et al. (2011) and Kimball et al. (2014) suggests that different species of gorgonian calcitic corals fractionate oxygen and carbon following similar mechanisms. Based on the highly significant $\delta^{18}O_{intercept}$ vs. temperature relationship, the "lines technique" method can be reliably applied to the calcitic skeleton to obtain calcification temperature estimates in the past, although this approach requires the knowledge of the past $\delta^{18}O$ and $\delta^{13}C$ composition of seawater and it is labor and time intensive. However, the advantage of this method when applied to live-collected and fossil *C. rubrum* and more in general to calcitic corals is that it can potentially provide decadal to centennial time series of seawater temperature at annual resolution. This can be done by micromilling multiple sub-samples along growth bands and reasonably assuming stable seawater $\delta^{18}O$ and $\delta^{13}C$ for the past decades to the last 100 years. Finally, the "lines technique" method applied to calcitic corals could be combined with the estimates of past seawater temperature based on the geochemical composition (e.g. Sr/Ca, Li/Mg) of coeval aragonitic corals to potentially reconstruct variations in seawater $\delta^{18}O$ and eventually salinity in regions, like the Mediterranean, where a well-defined $\delta^{18}O$-salinity relationship exists (Pierre, 1999).

Conclusions

The skeleton of four specimens of the Mediterranean slow-growing coral *C. rubrum* collected in the north-western Mediterranean Sea between 15 and 50 m water depth was investigated for growth ring counting (age determination) and stable isotopes. The ring thickness varies in the annular zone from 56 μm/yr for the specimen collected in the Medes Islands to 118 μm/yr for the deeper sample from Portofino. The values of the mean growth rate calculated for the entire diameter (Table 2) are similar to previous findings for the same coral species. The micromill $\delta^{13}C$ and $\delta^{18}O$ values show a strong fine-scale variability, with the internal medullar zone being generally depleted in ^{18}O and ^{13}C compared to the external annular portion. There is also a significant isotopic difference between the branch and the basal stem of the coral. All the coral portions are characterized by $\delta^{18}O$ and $\delta^{13}C$ values shifted from the expected oxygen and carbon equilibrium values for inorganically-precipitated calcite, suggesting a strong kinetic and/or physiological control during the skeletal formation. The $\delta^{18}O$ and $\delta^{13}C$ values show highly significant positive linear correlations that were used to calculate the $\delta^{18}O_{intercept}$ relationship with temperature, following the "lines technique" method developed by Smith et al. (2000) for aragonitic corals. A general calibration equation was obtained by combining our data with those published by Hill et al. (2011) and Kimball et al. (2014), extending the previous calibrations for calcitic corals over a temperature range from 2°C and 17°C.

Acknowledgements

This work is part of the European project MedSeA (Mediterranean Sea Acidification in a Changing Climate, #265103). Thin sections were prepared with the kind help of Luis Gordon at UAB, Spain, and Birgit Leipner-Mata at GZN, Germany. We are grateful to Joaquim Garrabou and Nathaniel Bensoussan to kindly provide temperature data from TMEDnet network. We appreciate the fruitful discussion with P.G. Mortyn and M. Grelaud. We are thankful for the constructive comments and suggestions of F.J. Millero and the two anonymous reviewers that improved the manuscript. We are grateful for the financial support of the MISTRALS-PaleoMeX and ENVIMED projects. This article is an ISMAR-CNR Bologna and contributing to the ICTA 'Unit of Excellence' (MinECo, MDM2015-0552) and to the AGAUR Generalitat de Catalunya (MERS, 2014 SGR - 1356).

References

Adkins, J.F., Boyle, E.A., Curry, W.B., Lutringer, A., 2003. Stable isotopes in deep-sea corals and a new mechanism for "vital effects." Geochim. Cosmochim. Acta 67, 1129–1143. doi:10.1016/S0016-7037(00)01203-6

Bavestrello, G., Bonito, M., Sarà, M., 1993. Influence of depth on the size of sponge spicules. Sci. Mar. 57, 415–420.

Bayer, F.M., Cairns, S.D., 2003. A new genus of the scleraxonian family Coralliidae

(Octocorallia: Gorgonacea). Proc. Biol. Soc. Washingt. 116, 222–228.
Bemis, B.E., Spero, H.J., Bijma, J., Lea, D.W., 1998. Reevaluation of the oxygen isotopic composition of planktonic foraminifera: Experimental results and revised paleotemperature equations. Paleoceanography 13, 150–160. doi:10.1029/98PA00070
Benedetti, M.C., Priori, C., Erra, F., Santangelo, G., 2016. Growth patterns in mesophotic octocorals: Timing the branching process in the highly-valuable Mediterranean *Corallium rubrum*. Estuar. Coast. Shelf Sci. 171, 106–110. doi:10.1016/j.ecss.2015.12.026
Bensoussan, N., Romano, J.C., Harmelin, J.G., Garrabou, J., 2010. High resolution characterization of northwest Mediterranean coastal waters thermal regimes: To better understand responses of benthic communities to climate change. Estuar. Coast. Shelf Sci. 87, 431–441. doi:10.1016/j.ecss.2010.01.008
Bevington, P.R., Robinson, D.K., 1992. Data Reduction and Error Analysis for The Physical Sciences, 2nd ed. McGraw-Hill Companies, New York.
Boyer, T.P., Antonov, J.I., Baranova, O.K., Coleman, C., Garcia, H.E., Grodsky, A., Johnson, D.R., Locarnini, R.A., Mishonov, A.V., O'Brien, T.D., Paver, C.R., Reagan, J.R., Seidov, D., Smolyar, I.V., Zweng, M.M., 2013. World Ocean Database 2013. Levitus, S., Mishonoc, A. (Eds.), NOAA Atlas NESDIS 72, World Ocean Database 2013, 209 pp. doi: 10.7289/V5NZ85MT
Bramanti, L., Vielmini, I., Rossi, S., Tsounis, G., Iannelli, M., Cattaneo-Vietti, R., Priori, C., Santangelo, G., 2014. Demographic parameters of two populations of red coral (*Corallium rubrum* L. 1758) in the North Western Mediterranean. Mar. Biol. 161, 1015–1026. doi:10.1007/s00227-013-2383-5
Cattaneo-Vietti, R., Cicogna, F., 1993. Il corallo rosso in Mediterraneo: Arte, storia e scienza. [Red coral in the Mediterranean sea: art, history and science]. Ministero delle Politiche Agricole, Alimentari e Forestali, Roma : Massa Lubrense, 3-9.
Chintiroglou, H., Dounas, C., Koukouras, A., 1989. The Presence of *Corallium rubrum* (Linnaeus, 1758) in the Eastern Mediterranean Sea. Mitteilungen aus dem Zool. Museum Berlin 65, 145–149. doi:10.1002/mmnz.19890650106
Epstein, S., Buchsbaum, R., Lowenstam, H.A., Urey, H.C., 1953. Revised carbonate-water isotopic temperature scale. Geol. Soc. Am. Bull. 64, 1315–1325. doi:10.1130/0016-7606(1953)64
Gagan, M.K., Ayliffe, L.K., Beck, J.W., Cole, J.E., Druffel, E.R.M., Dunbar, R.B., Schrag, D.P., 2000. New views of tropical paleoclimates from corals. Quat. Sci. Rev. 19, 45–64. doi:10.1016/S0277-3791(99)00054-2
Gagan, M.K., Chivas, A.R., Isdale, P.J., 1994. High-resolution isotopic records from corals using ocean temperature and mass-spawning chronometers. Earth Planet. Sci. Lett. 121, 549–558. doi:10.1016/0012-821X(94)90090-6
Garrabou, J., Harmelin, J.G., 2002. A 20-year study on life-history traits of a harvested long-lived temperate coral in the NW Mediterranean: insights into conservation and management needs. J. Anim. Ecol. 71, 966–978.
Grossman, E.L., Ku, T.-L., 1986. Oxygen and carbon isotope fractionation in biogenic aragonite: Temperature effects. Chem. Geol. 59, 59–74. doi:10.1016/0168-9622(86)90057-6
Hill, T.M., LaVigne, M., Spero, H.J., Guilderson, T., Gaylord, B., Clague, D., 2012. Variations in seawater Sr/Ca recorded in deep-sea bamboo corals. Paleoceanography 27, 5–11. doi:10.1029/2011PA002260
Hill, T.M., Spero, H.J., Guilderson, T., Lavigne, M., Clague, D., MacAlello, S., Jang, N., 2011. Temperature and vital effect controls on bamboo coral (Isididae) isotope geochemistry: A test of the “lines method.” Geochemistry, Geophys. Geosystems 12, 1–

14. doi:10.1029/2010GC003443

Kim, S.-T., O'Neil, J.R., 1997. Equilibrium and nonequilibrium oxygen isotope effects in synthetic carbonates. Geochim. Cosmochim. Acta 61, 3461–3475. doi:10.1016/S0016-7037(97)00169-5

Kim, S.-T., O'Neil, J.R., Hillaire-Marcel, C., Mucci, A., 2007. Oxygen isotope fractionation between synthetic aragonite and water: Influence of temperature and Mg^{2+} concentration. Geochim. Cosmochim. Acta 71, 4704–4715. doi:10.1016/j.gca.2007.04.019

Kimball, J.B., Dunbar, R.B., Guilderson, T.P., 2014. Oxygen and carbon isotope fractionation in calcitic deep-sea corals: Implications for paleotemperature reconstruction. Chem. Geol. 381, 223–233. doi:10.1016/j.chemgeo.2014.05.008

Leder, J.J., Swart, P.K., Szmant, A.M., Dodge, R.E., 1996. The origin of variations in the isotopic record of scleractinian corals: II. Carbon. Geochim. Cosmochim. Acta 60, 2871–2885. doi:10.1016/0016-7037(96)00119-6

LeGrande, A.N., Schmidt, G.A., 2006. Global gridded data set of the oxygen isotopic composition in seawater. Geophys. Res. Lett. 33, L12604. doi:10.1029/2006GL026011

Linares, C., Cebrian, E., Kipson, S., Garrabou, J., 2013. Does thermal history influence the tolerance of temperate gorgonians to future warming? Mar. Env. Res. 89, 45–52. doi:10.1016/j.marenvres.2013.04.009

Linnaeus, C., 1758. Systema naturae per regna tria naturae, secundum classes, ordines, genera, species, cum characteribus, differentiis, synonymis, locis. Regnum Animale, 10th ed. Lipsiae.

López Correa, M., Montagna, P., Vendrell-Simón, B., McCulloch, M., Taviani, M., 2010. Stable isotopes ($\delta^{18}O$ and $\delta^{13}C$), trace and minor element compositions of Recent scleractinians and Last Glacial bivalves at the Santa Maria di Leuca deep-water coral province, Ionian Sea. Deep-Sea Res. Part II Top. Stud. Oceanogr. 57, 471–486. doi:10.1016/j.dsr2.2009.08.016

Marschal, C., Garrabou, J., Harmelin, J.G., Pichon, M., 2004. A new method for measuring growth and age in the precious red coral *Corallium rubrum* (L.). Coral Reefs 23, 423–432. doi:10.1007/s00338-004-0398-6

McConnaughey, T., 1989. ^{13}C and ^{18}O isotopic disequilibrium in biological carbonates: II. *In vitro* simulation of kinetic isotope effects. Geochim. Cosmochim. Acta 53, 163–171. doi:10.1016/0016-7037(89)90283-4

McCulloch, M.T., Tudhope, A.W., Esat, T.M., Mortimer, G.E., Chappell, J., Pillans, B., Chivas, A.R., Omura, A., 1999. Coral record of equatorial temperatures during the Penultimate Deglaciation at Huon Peninsula. Science 283, 202–204. doi:10.1126/science.283.5399.202

Millot, C., 1990. The Gulf of Lions' hydrodynamics. Cont. Shelf Res. 10, 885–894. doi:10.1016/0278-4343(90)90065-T

Millot, C., 1979. Wind induced upwellings in the Gulf of Lions. Oceanol. Acta 2, 261–274.

Mitsuguchi, T., Matsumoto, E., Abe, O., Uchida, T., Isdale, P.J., 1996. Mg/Ca Thermometry in coral skeletons. Science 274, 961–963. doi:10.1126/science.274.5289.961

Montagna, P., McCulloch, M., Douville, E., López Correa, M., Trotter, J., Rodolfo-Metalpa, R., Dissard, D., Ferrier-Pagès, C., Frank, N., Freiwald, A., Goldstein, S., Mazzoli, C., Reynaud, S., Rüggeberg, A., Russo, S., Taviani, M., 2014. Li/Mg systematics in scleractinian corals: Calibration of the thermometer. Geochim. Cosmochim. Acta 132, 288–310. doi:10.1016/j.gca.2014.02.005

Montagna, P., McCulloch, M., Mazzoli, C., Silenzi, S., Odorico, R., 2007. The non-tropical coral *Cladocora caespitosa* as the new climate archive for the Mediterranean: high-resolution (~weekly) trace element systematics. Quat. Sci. Rev. 26, 441–462. doi:10.1016/j.quascirev.2006.09.008

Montagna, P., McCulloch, M., Taviani, M., Mazzoli, C., Begona Vendrell, 2006. Phosphorus in cold-water corals as a proxy for seawater nutrient chemistry. Science 312, 1788–1791. doi:10.1126/science.1125781

Montagna, P., McCulloch, M., Taviani, M., Remia, A., Rouse, G., 2005. High-resolution trace and minor element compositions in deep-water scleractinian corals (*Desmophyllum dianthus*) from the Mediterranean Sea and the Great Australian Bight. In: Freiwald, A., Roberts, J.M. (eds.) Cold-water corals and ecosystems. 1109–1126, Springer, Heidelberg. doi:10.1007/3-540-27673-4

Pelejero, C., Calvo, E., McCulloch, M.T., Marshall, J.F., Gagan, M.K., Lough, J.M., Opdyke, B.N., 2005. Preindustrial to modern interdecadal variability in coral reef pH. Science 309, 2204–2207. doi:10.1126/science.1113692

Petrenko, A.A., 2003. Variability of circulation features in the Gulf of Lion NW Mediterranean Sea. Importance of inertial currents. Oceanol. Acta 26, 323–338. doi:10.1016/S0399-1784(03)00038-0

Pierre, C., 1999. The oxygen and carbon isotope distribution in the Mediterranean water masses. Mar. Geol. 153, 41–55. doi:10.1016/S0025-3227(98)00090-5

Roark, E.B., Guilderson, T.P., Flood-Page, S., Dunbar, R.B., Ingram, B.L., Fallon, S.J., McCulloch, M., 2005. Radiocarbon-based ages and growth rates of bamboo corals from the Gulf of Alaska. Geophys. Res. Lett. 32, 1–5. doi:10.1029/2004GL021919

Robinson, L.F., Adkins, J.F., Frank, N., Gagnon, A.C., Prouty, N.G., Roark, E.B., Van de Flierdt, T., 2014. The geochemistry of deep-sea coral skeletons: A review of vital effects and applications for palaeoceanography. Deep-Res. Part II Top. Stud. Oceanogr. 99, 184–198. doi:10.1016/j.dsr2.2013.06.005

Romanek, C.S., Grossman, E.L., Morse, J.W., 1992. Carbon isotopic fractionation in synthetic aragonite and calcite: Effects of temperature and precipitation rate. Geochim. Cosmochim. Acta 56, 419–430. doi:10.1016/0016-7037(92)90142-6

Rossi, S., Tsounis, G., Orejas, C., Padrón, T., Gili, J.M., Bramanti, L., Teixidó, N., Gutt, J., 2008. Survey of deep-dwelling red coral (*Corallium rubrum*) populations at Cap de Creus (NW Mediterranean). Mar. Biol. 154, 533–545. doi:10.1007/s00227-008-0947-6

Salat, J., Pascual, J., 2002. The oceanographic and meteorological station at l'Estartit (NW Mediterranean), in: Commission Internationale Pour l'Exploration Scientifique de La Mer Méditerranée Workshop Series ''Tracking Long-Term Hydrological Change in the Mediterranean Sea. pp. 533–545.

Schneider, C.A., Rasband, W.S., Eliceiri, K.W., 2012. NIH Image to ImageJ: 25 years of image analysis. Nat. Methods 9, 671–675. doi:10.1038/nmeth.2089

Shackleton, N.J., 1974. Attainment of isotopic equilibrium between ocean water and the benthonic foraminifera genus *Uvigerina*: isotopic changes in the ocean during the last glacial. In: (Les méthodes quantitatives d'étude des varitions du climat au cours du pléistocène), Colloq. Int. du C.N.R.S 219, 203–209.

Sherwood, O.A., Edinger, E.N., 2009. Ages and growth rates of some deep-sea gorgonian and antipatharian corals of Newfoundland and Labrador. Can. J. Fish. Aquat. Sci. 66, 142–152. doi:10.1139/F08-195

Sherwood, O.A., Edinger, E.N., Guilderson, T.P., Ghaleb, B., Risk, M.J., Scott, D.B., 2008. Late Holocene radiocarbon variability in Northwest Atlantic slope waters. Earth Planet. Sci. Lett. 275, 146–153. doi:10.1016/j.epsl.2008.08.019

Sherwood, O.A., Scott, D.B., Risk, M.J., Guilderson, T.P., 2005. Radiocarbon evidence for annual growth rings in the deep-sea octocoral *Primnoa resedaeformis*. Mar. Ecol. Prog. Ser. 301, 129–134. doi:10.3354/meps301129

Sinclair, D.J., Williams, B., Allard, G., Ghaleb, B., Fallon, S., Ross, S.W., Risk, M., 2011. Reproducibility of trace element profiles in a specimen of the deep-water bamboo coral

Keratoisis sp. Geochim. Cosmochim. Acta 75, 5101–5121. doi:10.1016/j.gca.2011.05.012
Smith, J.E., Schwarcz, H.P., Risk, M.J., 2000. Paleotemperatures from deep-sea corals: overcoming “vital effects". Palaios 15, 25–32.
Taviani, M., 1997. L'uomo ed il corallo. Cat. Ori delle Alpi, Trento 151–152.
Taviani, M., Angeletti, L., Antolini, B., Ceregato, A., Froglia, C., López Correa, M., Montagna, P., Remia, F., Trincardi, F., Vertino, A., 2011. Geo-biology of Mediterranean Deep-Water Coral Ecosystems. Mar. Res. CNR 6, 705–719.
Tescione, G., 1973. The italians and their coral fishing. Fausto Fiorentino, Napoli, p. 490.
Thresher, R., Rintoul, S.R., Koslow, J.A., Weidman, C., Adkins, J., Proctor, C., 2004. Oceanic evidence of climate change in southern Australia over the last three centuries. Geophys. Res. Lett. 31, 2–5. doi:10.1029/2003GL018869
Thresher, R.E., MacRae, C.M., Wilson, N.C., Fallon, S., 2009. Feasibility of age determination of deep-water bamboo corals (Gorgonacea; Isididae) from annual cycles in skeletal composition. Deep-Sea Res. Part I Oceanogr. Res. Pap. 56, 442–449. doi:10.1016/j.dsr.2008.10.003
Tracey, D.M., Neil, H., Marriott, P., Andrews, A.H., Cailliet, G.M., Sanchez, J.A., 2007. Age and growth of two genera of deep-sea bamboo corals (family Isididae) in New Zealand waters. Bull. Mar. Sci. 81, 393–408.
Tsounis, G., Rossi, S., Gili, J.-M., Arntz, W., 2006. Population structure of an exploited benthic cnidarian: the case study of red coral (*Corallium rubrum* L.). Mar. Biol. 149, 1059–1070. doi:10.1007/s00227-006-0302-8
Tsounis, G., Rossi, S., Gili, J.M., Arntz, W.E., 2007. Red coral fishery at the Costa Brava (NW Mediterranean): Case study of an overharvested precious coral. Ecosystems 10, 975–986. doi:10.1007/s10021-007-9072-5
Vertino, A., Savini, A., Rosso, A., Di Geronimo, I., Mastrototaro, F., Sanfilippo, R., Gay, G., Etiope, G., 2010. Benthic habitat characterization and distribution from two representative sites of the deep-water SML Coral Province (Mediterranean). Deep-Sea Res. Part II Top. Stud. Oceanogr. 57, 380–396. doi:10.1016/j.dsr2.2009.08.023
Vielzeuf, D., Garrabou, J., Gagnon, A., Ricolleau, A., Adkins, J., Günther, D., Hametner, K., Devidal, J.L., Reusser, E., Perrin, J., Floquet, N., 2013. Distribution of sulphur and magnesium in the red coral. Chem. Geol. 355, 13–27. doi:10.1016/j.chemgeo.2013.07.008
Yoshimura, T., Suzuki, A., Iwasaki, N., 2015. Mechanism of O and C isotope fractionation in magnesian calcite skeletons of Octocorallia corals and an implication on their calcification response to ocean acidification. Biogeosciences Discuss. 12, 389–412. doi:10.5194/bgd-12-389-2015
Younes, W.A.N., Bensoussan, N., Romano, J.-C., Arlhac, D., Lafont, M.-G., 2003. Seasonal and interannual variations (1996-2000) of the coastal waters east of the Rhone river mouth as indicated by the SORCOM series. Oceanol. Acta 26, 311–321. doi:10.1016/S0399-1784(03)00037-9
Zibrowius, H., Monteiro Marques, V., Grasshoff, M., 1984. La répartition du *Corallium rubrum* dans l'Atlantique (Cnidaria: Anthozoa: Gorgonaria). Tethys 11, 163–170.
Ziveri, P., Stoll, H., Probert, I., Klaas, C., Geisen, M., Ganssen, G., Young, J., 2003. Stable isotope 'vital effects' in coccolith calcite. Earth Planet. Sci. Lett. 210, 137–149. doi:10.1016/S0012-821X(03)00101-8
Ziveri, P., Thoms, S., Probert, I., Geisen, M., Langer, G., 2012. A universal carbonate ion effect on stable oxygen isotope ratios in unicellular planktonic calcifying organisms. Biogeosciences 9, 1025–1032. doi:10.5194/bg-9-1025-2012

Figure Captions

Fig. 1. Map with the locations of the *C. rubrum* specimen analyzed. Four colonies have been retrieved by scuba diving from the shallow water (between 15 to 50 m depth) of Riou Island, Medes Islands (Spain), Scandola (Corsica) and Portofino (Italy).

Fig. 2. Mean monthly temperatures sourced from the NOAA NODC WOA13 (0.25° grid) Database (Boyer et al., 2013) (from 1955 to 2012) and the T-MedNet network (from 2004 to 2014).

Fig. 3. Toluidine blue stained thinsection of *C. rubrum* from Medes Islands under the stereomicroscope. The annual growth pattern in the basal stem are visible as alternating dark and light bands.

Fig. 4. *C. rubrum* colony from Riou Island (A). Position of the micromill tracks across the entire branches and bases (B to E). These tracks for stable isotope sampling are oriented parallel to the growth increments. (B) Tracks (RI-1 to RI-44) on the branch of the Riou Island sample, (C) Tracks (CO-1 to CO-35) on the branch of the Corsica sample, (D) Tracks (MI-1 to MI-72) on the base of the Medes Island sample, and (E) Tracks (PF-1 to PF-86) on the base of the Portofino sample.

Fig. 5. Coral $\delta^{18}O$ (grey circles) and $\delta^{13}C$ (white circles) values plotted against the linear micromill distance from the outer edge of the skeleton for the samples PF (A), MI (B), RI (C) and CO (D) as well as the linear regressions of $\delta^{18}O$ vs. $\delta^{13}C$ (rectangles: medullar zone; black circles: annular zone; solid grey line: linear regression for all the data; solid black line: linear regression for the annular zone; dashed line: linear regression for the medullar zone). The micro-gram sub-samples for stable isotopes were obtained using a Merchantek Micromill (New Wave) across longitudinal stem sections (see Fig. 4). Arrows indicate growth direction from the central axial portion (medullar) towards the outer edge of the coral. Large rectangles indicate the sub-samples within the medullar zone.

Fig. 6. $\delta^{18}O$ and $\delta^{13}C$ values obtained from the basal stems (rectangles: MI; triangles: PF) and from the branches (crosses: RI; circles: CO).

Fig. 7. $\delta^{18}O$-$\delta^{13}C$ linear regressions for (A) RI, (B) MI, (C) CO, and (D) PF samples. (rectangles: medullar zone; circles: annular zone). Grey and white symbols represent values obtained from the two different sides of the annular zone (dashed line: linear regression for the medullar zone; solid lines: linear regressions for the annular zones).

Fig. 8. Linear regressions (with 95% confidence intervals) of $\delta^{18}O_{intercept}$ values vs. ambient seawater temperature obtained by combining the data from this study (A) calculated from the full data or (B) from selected data, with the data by Kimball et al. (2014) and Hill et al. (2011) (red envelope: 95% confidence interval for the regression line calculated using all the data; blue envelope: 95% confidence interval for the regression line calculated using a selection of the data, see discussion; yellow envelope: 95% confidence interval for the regression line of Kimball et al. (2014)). The regression lines are compared with the calcite–water fractionation curve determined by Bemis et al. (1998) and Shackleton, (1974), and aragonite–water fractionation curve by Grossman and Ku (1986).

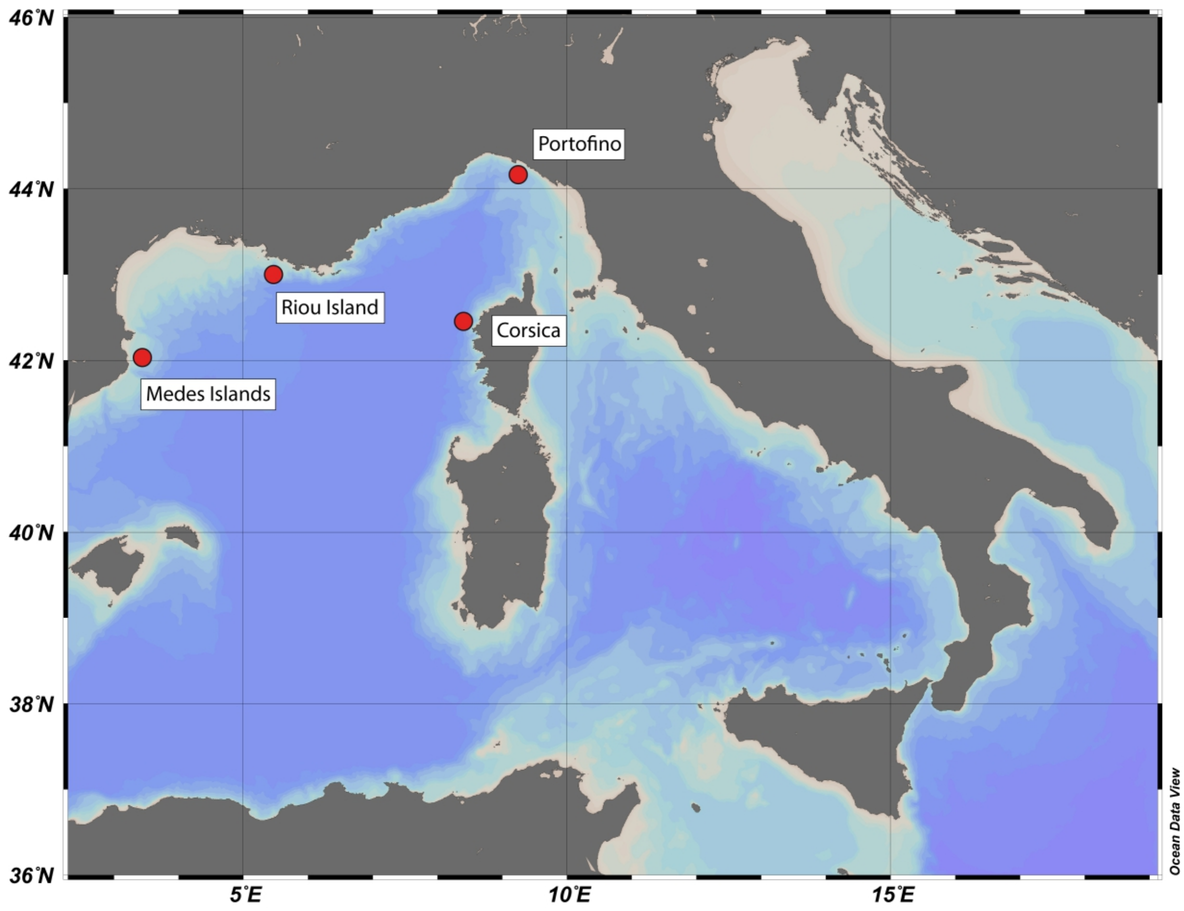
46°N
44°N
42°N
40°N
38°N
36°N
5°E
10°E
15°E
Portofino
Riou Island
Corsica
Medes Islands
Ocean Data View

Fig. 1

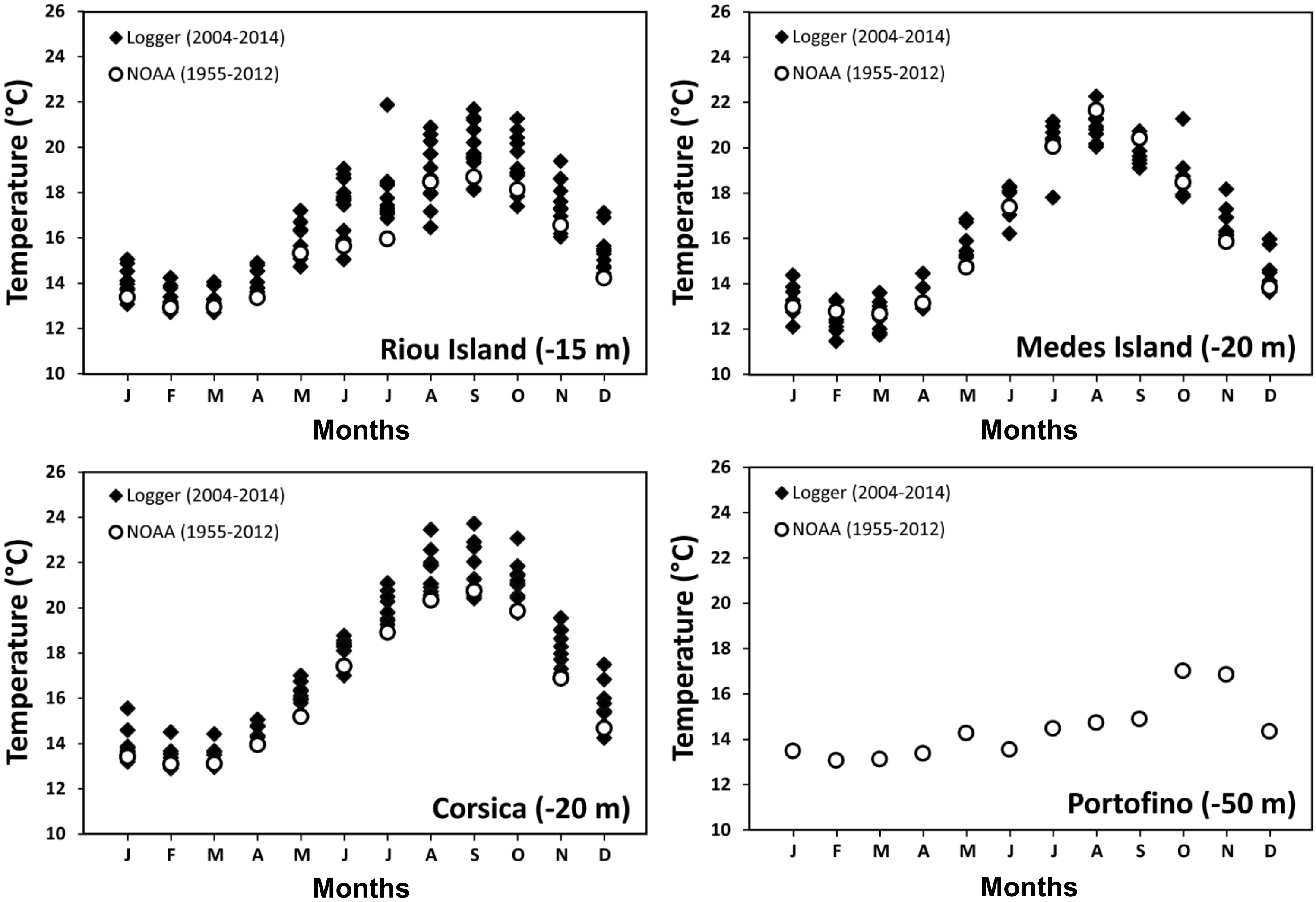
Logger (2004-2014)
NOAA (1955-2012)
Temperature (°C)
Months
J F M A M J J A S O N D
Riou Island (-15 m)
Medes Island (-20 m)
Corsica (-20 m)
Portofino (-50 m)

Fig. 2

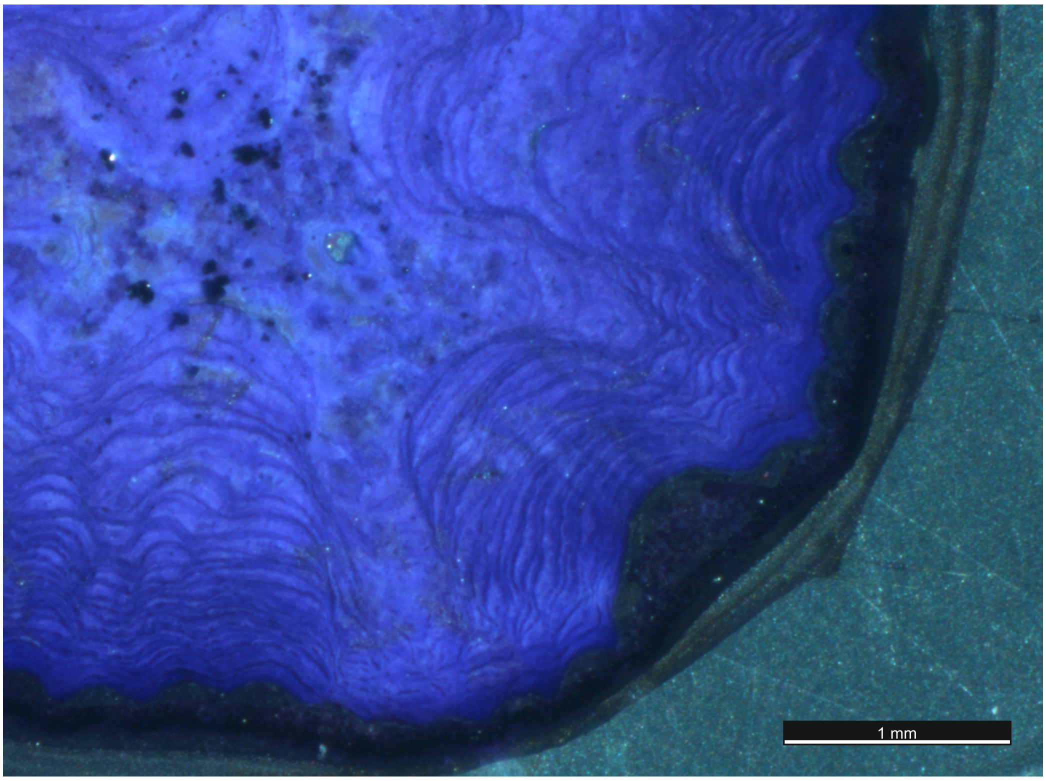

Fig. 3

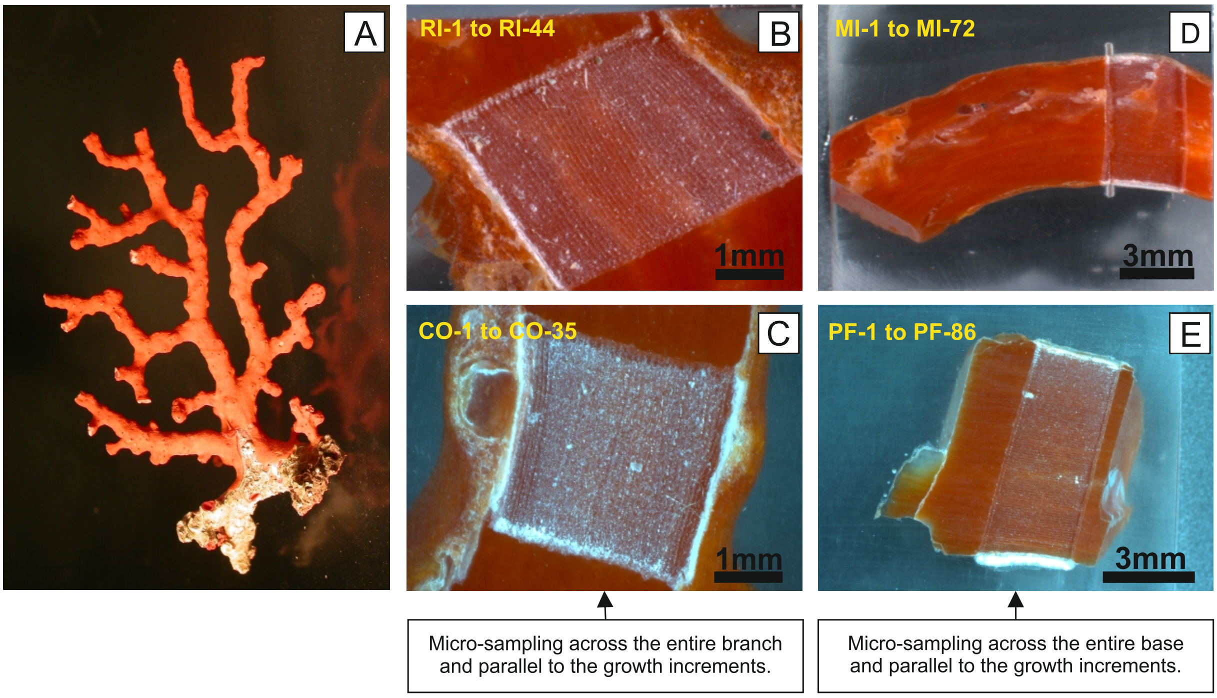
A
RI-1 to RI-44
B
1mm
MI-1 to MI-72
D
3mm
CO-1 to CO-35
C
1mm
PF-1 to PF-86
E
3mm
Micro-sampling across the entire branch and parallel to the growth increments.
Micro-sampling across the entire base and parallel to the growth increments.

Fig. 4

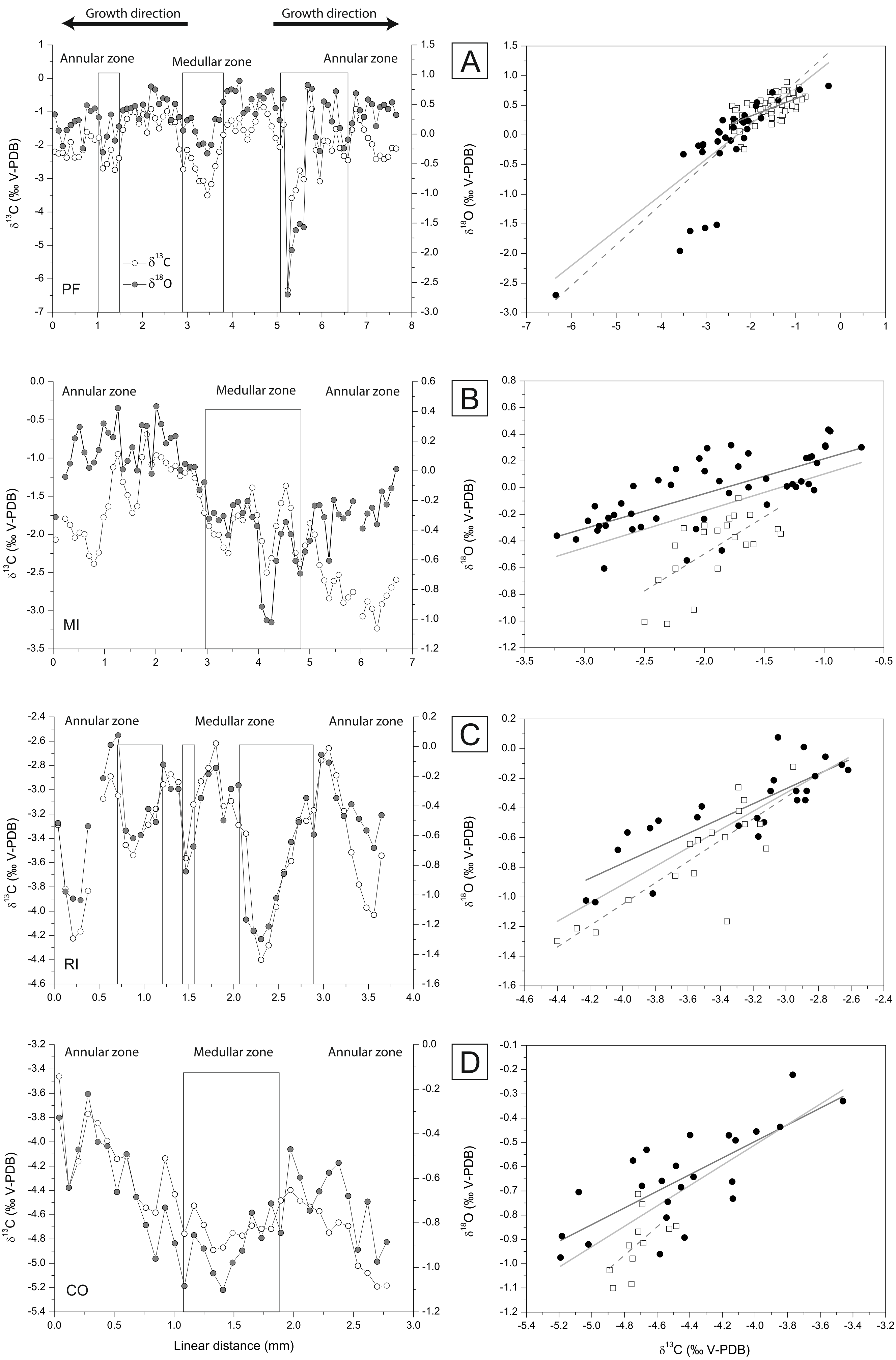

Growth direction
Growth direction
Annular zone
Medullar zone
Annular zone
A
B
C
D
PF
MI
RI
CO
δ13C
δ18O
δ13C (‰ V-PDB)
δ18O (‰ V-PDB)
Linear distance (mm)

Fig. 5

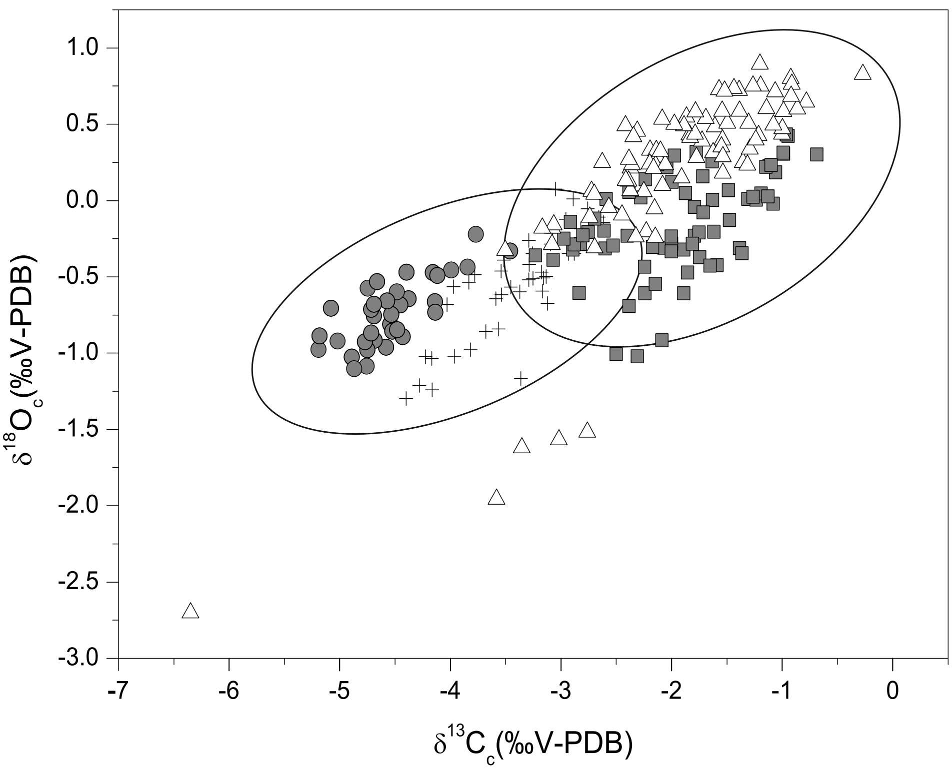

Fig. 6

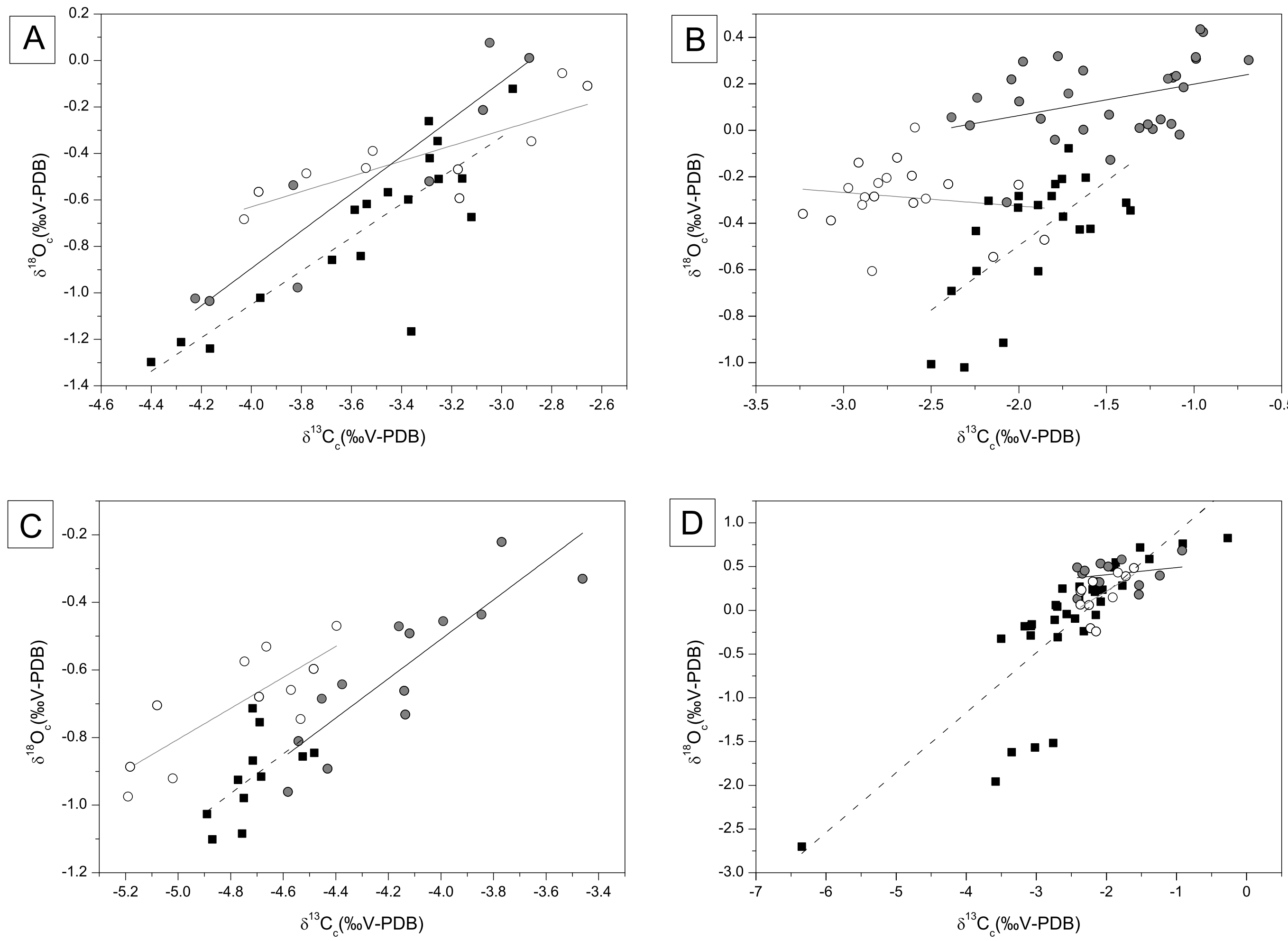

Fig. 7

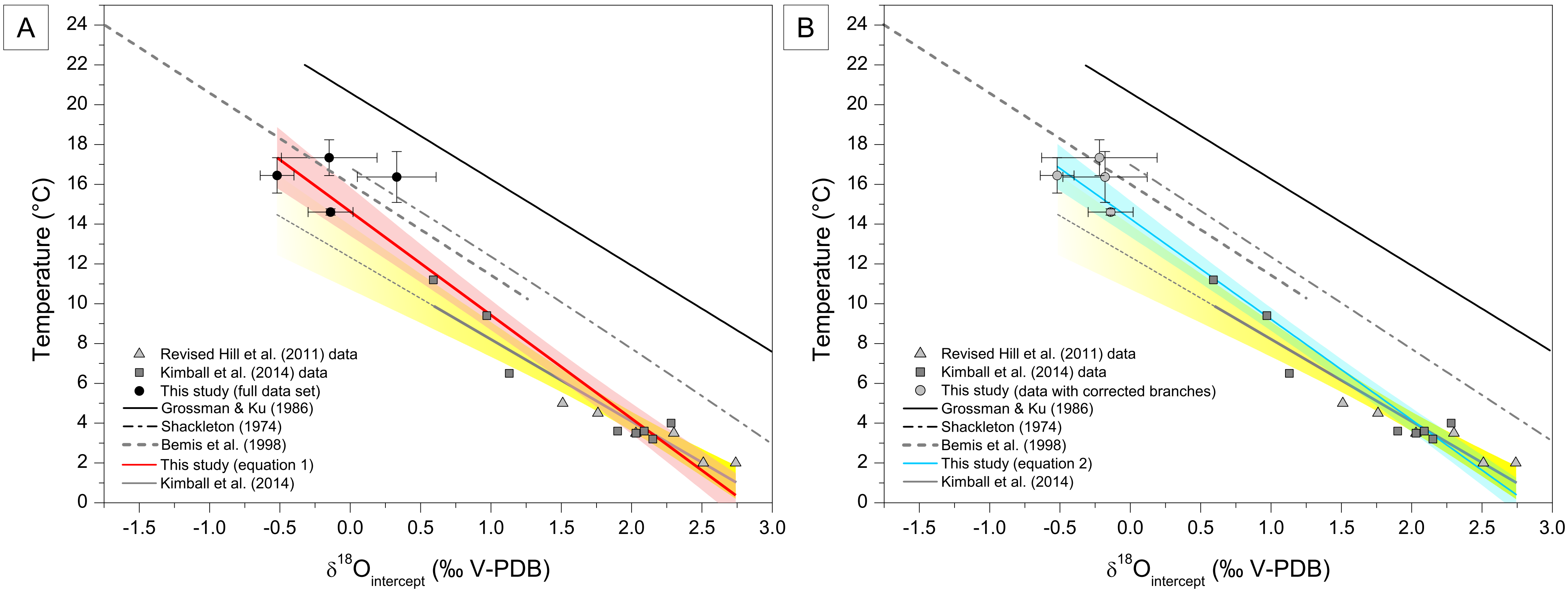
A
B
Temperature (°C)
δ18O intercept (‰ V-PDB)
Revised Hill et al. (2011) data
Kimball et al. (2014) data
This study (full data set)
This study (data with corrected branches)
Grossman & Ku (1986)
Shackleton (1974)
Bemis et al. (1998)
This study (equation 1)
This study (equation 2)
Kimball et al. (2014)

Fig. 8

Tab.1. Sampling locations of live-collected *Corallium rubrum* specimens from the Mediterranean Sea.

Sample	Sampling Location	Depth (m)	Latitude	Longitude	Date of sampling	Temperature (°C)	Salinity (psu)[b]	$\delta^{18}O_{sw}$ (‰ V-SMOW)[c]	$\delta^{13}C_{DIC}$ (‰ V-PDB)[d]
RI (Branch)	Riou Island, France	15	43°11'N	05°23'E	06/2008	16.37 ± 1.28 [a]	38.009 ± 0.020	1.31 ± 0.017	0.80
CO (Branch)	Scandola Palazzu, Corsica, France	21	42°21'N	08°32'E	07/07/2008	17.34 ± 0.90 [a]	37.929 ± 0.048	1.34 ± 0.017	0.90
PF (Base)	Portofino, Italy	50	44°18'N	09°13'E	05/2009	14.61 ± 0.16 [b]	38.015 ± 0.011	1.39 ± 0.006	1.20 ± 0.22
MI (Base)	Medes Islands, Spain	18	42°02'N	03°13'E	27/06/2008	16.45 ± 0.89 [a]	37.748 ± 0.058	1.31 ± 0.019	1.20 ± 0.22

[a] Temperature values are sourced from T-MedNet network (www.t-mednet.org)
[b] Temperature and Salinity values are sourced from NOAA NODC WOA13 (0.25° grid) Database (Boyer et al., 2013).
[c] Data from NASA GISS LeGrande_Schmidt2006 v1p1 $\delta^{18}O$ (Grid-1x1).
[d] Data from Pierre (1999).

Tab.2. Sampling depth, mean seawater temperature, diameter and age estimation of PF, MI and RI specimens. Growth rate values (mean ± 1SD) represent the average of the growth rates calculated from different transects in the annular zone.

Sample	Depth (m)	Mean T (°C)	Diameter (mm)	Age estimation (year)	Growth rate in the annular zone (µm/yr)	Mean growth rate (µm/yr)
RI	15	16.37 ± 1.28	4.25	18 ± 2	85 ± 12	236 ± 27
MI	18	16.45 ± 0.89	5.16	30 ± 1	56 ± 6	172 ± 7
PF	50	14.61 ± 0.16	7.44	27 ± 6	118 ± 3	276 ± 65

Tab.3. Isotope data ($\delta^{13}C$ and $\delta^{18}O$)[a] for the Mediterranean red coral *Corallium rubrum.*

Sample	Linear distance (mm)	$\delta^{13}C$ (‰V-PDB)	$\delta^{18}O$ (‰V-PDB)	Sample	Linear distance (mm)	$\delta^{13}C$ (‰V-PDB)	$\delta^{18}O$ (‰V-PDB)	Sample	Linear distance (mm)	$\delta^{13}C$ (‰V-PDB)	$\delta^{18}O$ (‰V-PDB)	Sample	Linear distance (mm)	$\delta^{13}C$ (‰V-PDB)	$\delta^{18}O$ (‰V-PDB)
PF-1	0.045	-2.20	0.33	MI-1	0.047	-2.07	-0.31	CO-1	0.040	-3.46	-0.33	RI-1	0.04	-3.29	-0.52
PF-2	0.134	-2.25	0.06	MI-2	0.140	-	-	CO-2	0.121	-4.38	-0.64	RI-2	0.13	-3.82	-0.98
PF-3	0.224	-2.23	-0.20	MI-3	0.234	-1.79	-0.04	CO-3	0.201	-4.16	-0.47	RI-3	0.21	-4.22	-1.02
PF-4	0.313	-2.37	0.07	MI-4	0.327	-1.88	0.05	CO-4	0.282	-3.77	-0.22	RI-4	0.29	-4.17	-1.04
PF-5	0.403	-1.91	0.15	MI-5	0.421	-2.04	0.22	CO-5	0.362	-3.85	-0.44	RI-5	0.38	-3.83	-0.54
PF-6	0.492	-2.37	0.21	MI-6	0.514	-1.98	0.30	CO-6	0.443	-3.99	-0.46	RI-6	0.46	-	-
PF-7	0.582	-2.36	0.23	MI-7	0.608	-2.00	0.12	CO-7	0.523	-4.14	-0.66	RI-7	0.54	-3.07	-0.21
PF-8	0.671	-2.15	-0.24	MI-8	0.701	-2.28	0.02	CO-8	0.604	-4.12	-0.49	RI-8	0.63	-2.89	0.01
PF-9	0.761	-1.61	0.48	MI-9	0.795	-2.38	0.06	CO-9	0.684	-4.45	-0.68	RI-9	0.71	-3.05	0.08
PF-10	0.850	-1.73	0.39	MI-10	0.888	-2.24	0.14	CO-10	0.765	-4.54	-0.81	**RI-10**	**0.80**	**-3.45**	**-0.57**
PF-11	0.940	-1.84	0.43	MI-11	0.982	-1.78	0.32	CO-11	0.845	-4.58	-0.96	**RI-11**	**0.88**	**-3.54**	**-0.62**
PF-12	**1.029**	**-1.77**	**0.28**	MI-12	1.075	-1.63	0.26	CO-12	0.926	-4.14	-0.73	**RI-12**	**0.96**	**-3.37**	**-0.60**
PF-13	**1.119**	**-2.70**	**-0.31**	MI-13	1.169	-1.12	0.23	CO-13	1.006	-4.43	-0.89	**RI-13**	**1.05**	**-3.29**	**-0.42**
PF-14	**1.208**	**-2.57**	**-0.04**	MI-14	1.262	-0.95	0.42	**CO-14**	**1.087**	**-4.76**	**-1.08**	**RI-14**	**1.13**	**-3.16**	**-0.51**
PF-15	**1.298**	**-2.14**	**0.33**	MI-15	1.356	-1.31	0.01	**CO-15**	**1.167**	**-4.53**	**-0.86**	**RI-15**	**1.22**	**-2.96**	**-0.12**
PF-16	**1.387**	**-2.74**	**-0.11**	MI-16	1.449	-1.48	0.07	**CO-16**	**1.248**	**-4.68**	**-0.92**	RI-16	1.30	-2.87	-0.29
PF-17	**1.477**	**-2.39**	**0.13**	MI-17	1.543	-1.72	0.16	**CO-17**	**1.328**	**-4.89**	**-1.03**	RI-17	1.38	-2.94	-0.29
PF-18	1.566	-1.54	0.40	MI-18	1.636	-1.63	0.00	**CO-18**	**1.409**	**-4.87**	**-1.10**	**RI-18**	**1.47**	**-3.56**	**-0.84**
PF-19	1.656	-1.21	0.43	MI-19	1.730	-0.99	0.31	**CO-19**	**1.489**	**-4.75**	**-0.98**	**RI-19**	**1.55**	**-3.12**	**-0.67**
PF-20	1.745	-1.00	0.44	MI-20	1.823	-0.69	0.30	**CO-20**	**1.570**	**-4.77**	**-0.92**	RI-20	1.63	-2.93	-0.35
PF-21	1.835	-1.00	0.47	MI-21	1.917	-1.08	-0.02	**CO-21**	**1.650**	**-4.69**	**-0.75**	RI-21	1.72	-2.82	-0.19
PF-22	1.924	-1.36	0.25	MI-22	2.010	-0.96	0.43	**CO-22**	**1.731**	**-4.72**	**-0.87**	RI-22	1.80	-2.62	-0.14
PF-23	2.014	-1.08	0.49	MI-23	2.104	-0.99	0.32	**CO-23**	**1.811**	**-4.72**	**-0.71**	RI-23	1.89	-3.13	-0.50
PF-24	2.103	-1.63	0.31	MI-24	2.197	-1.06	0.19	**CO-24**	**1.892**	**-4.48**	**-0.85**	RI-24	1.97	-3.09	-0.29
PF-25	2.193	-0.92	0.80	MI-25	2.291	-1.15	0.22	CO-25	1.972	-4.40	-0.47	**RI-25**	**2.05**	**-3.29**	**-0.26**
PF-26	2.282	-1.20	0.75	MI-26	2.384	-1.10	0.23	CO-26	2.053	-4.48	-0.60	**RI-26**	**2.14**	**-3.36**	**-1.17**
PF-27	2.372	-1.50	0.51	MI-27	2.478	-1.24	0.01	CO-27	2.133	-4.53	-0.74	**RI-27**	**2.22**	**-4.17**	**-1.24**
PF-28	2.461	-1.14	0.60	MI-28	2.571	-1.19	0.05	CO-28	2.214	-4.57	-0.66	**RI-28**	**2.30**	**-4.40**	**-1.30**
PF-29	2.551	-0.99	0.58	MI-29	2.665	-1.13	0.03	CO-29	2.294	-4.75	-0.57	**RI-29**	**2.39**	**-4.28**	**-1.21**

PF-30	2.640	-1.31	0.23	MI-30	2.758	-1.26	0.03	CO-30	2.375	-4.66	-0.53	**RI-30**	**2.47**	**-3.96**	**-1.02**
PF-31	2.730	-1.31	0.51	MI-31	2.852	-1.48	-0.13	CO-31	2.455	-4.69	-0.68	**RI-31**	**2.56**	**-3.68**	**-0.86**
PF-32	**2.819**	**-2.13**	**0.28**	**MI-32**	**2.945**	**-1.72**	**-0.08**	CO-32	2.536	-5.02	-0.92	**RI-32**	**2.64**	**-3.59**	**-0.64**
PF-33	**2.909**	**-2.72**	**0.06**	**MI-33**	**3.039**	**-1.89**	**-0.32**	CO-33	2.616	-5.08	-0.70	**RI-33**	**2.72**	**-3.25**	**-0.51**
PF-34	**2.998**	**-2.15**	**0.23**	**MI-34**	**3.132**	**-2.00**	**-0.28**	CO-34	2.697	-5.19	-0.97	**RI-34**	**2.81**	**-3.26**	**-0.35**
PF-35	**3.088**	**-2.39**	**0.27**	**MI-35**	**3.226**	**-2.00**	**-0.33**	CO-35	2.777	-5.18	-0.89	RI-35	2.89	-3.17	-0.59
PF-36	**3.177**	**-2.70**	**0.04**	**MI-36**	**3.319**	**-2.17**	**-0.30**					RI-36	2.97	-2.76	-0.05
PF-37	**3.267**	**-3.08**	**-0.18**	**MI-37**	**3.413**	**-2.25**	**-0.43**					RI-37	3.06	-2.66	-0.11
PF-38	**3.356**	**-3.06**	**-0.16**	**MI-38**	**3.506**	**-1.79**	**-0.23**					RI-38	3.14	-2.88	-0.35
PF-39	**3.446**	**-3.50**	**-0.32**	**MI-39**	**3.600**	**-1.75**	**-0.21**					RI-39	3.23	-3.18	-0.47
PF-40	**3.535**	**-3.17**	**-0.18**	**MI-40**	**3.693**	**-1.81**	**-0.28**					RI-40	3.31	-3.52	-0.39
PF-41	**3.625**	**-2.63**	**0.25**	**MI-41**	**3.787**	**-1.62**	**-0.20**					RI-41	3.39	-3.78	-0.49
PF-42	**3.714**	**-2.20**	**0.24**	**MI-42**	**3.880**	**-1.39**	**-0.31**					RI-42	3.48	-3.97	-0.57
PF-43	3.804	-1.69	0.54	**MI-43**	**3.974**	**-1.75**	**-0.37**					RI-43	3.56	-4.03	-0.68
PF-44	3.893	-1.39	0.72	**MI-44**	**4.067**	**-2.09**	**-0.92**					RI-44	3.65	-3.54	-0.46
PF-45	3.983	-1.26	0.75	**MI-45**	**4.161**	**-2.50**	**-1.01**								
PF-46	4.072	-1.57	0.73	**MI-46**	**4.254**	**-2.31**	**-1.02**								
PF-47	4.162	-1.20	0.89	**MI-47**	**4.348**	**-1.89**	**-0.61**								
PF-48	4.251	-1.55	0.35	**MI-48**	**4.441**	**-1.59**	**-0.42**								
PF-49	4.341	-1.83	0.41	**MI-49**	**4.535**	**-1.36**	**-0.35**								
PF-50	4.430	-1.54	0.59	**MI-50**	**4.628**	**-1.65**	**-0.43**								
PF-51	4.520	-1.29	0.34	**MI-51**	**4.722**	**-2.24**	**-0.61**								
PF-52	4.609	-0.78	0.65	**MI-52**	**4.815**	**-2.38**	**-0.69**								
PF-53	4.699	-0.86	0.60	MI-53	4.909	-2.15	-0.55								
PF-54	4.788	-1.06	0.71	MI-54	5.002	-1.85	-0.47								
PF-55	4.878	-1.44	0.73	MI-55	5.096	-2.00	-0.23								
PF-56	4.967	-1.79	0.44	MI-56	5.189	-2.40	-0.23								
PF-57	**5.057**	**-2.06**	**0.24**	MI-57	5.283	-2.60	-0.31								
PF-58	**5.146**	**-1.39**	**0.59**	MI-58	5.376	-2.84	-0.61								
PF-59	**5.236**	**-6.35**	**-2.70**	MI-59	5.470	-2.61	-0.20								

PF-60	**5.325**	**-3.58**	**-1.96**	MI-60	5.563	-2.53	-0.29
PF-61	**5.415**	**-3.35**	**-1.62**	MI-61	5.657	-2.89	-0.32
PF-62	**5.504**	**-2.76**	**-1.52**	MI-62	5.750	-2.82	-0.29
PF-63	**5.594**	**-3.02**	**-1.57**	MI-63	5.844	-2.75	-0.21
PF-64	**5.683**	**-0.27**	**0.83**	MI-64	5.937	-	-
PF-65	**5.773**	**-0.91**	**0.76**	MI-65	6.031	-3.07	-0.39
PF-66	**5.862**	**-2.15**	**-0.05**	MI-66	6.124	-2.88	-0.29
PF-67	**5.952**	**-3.08**	**-0.29**	MI-67	6.218	-2.97	-0.25
PF-68	**6.041**	**-1.87**	**0.55**	MI-68	6.311	-3.23	-0.36
PF-69	**6.131**	**-1.89**	**0.49**	MI-69	6.405	-2.92	-0.14
PF-70	**6.220**	**-2.16**	**0.21**	MI-70	6.498	-2.80	-0.23
PF-71	**6.310**	**-1.52**	**0.72**	MI-71	6.592	-2.69	-0.12
PF-72	**6.399**	**-2.08**	**0.10**	MI-72	6.685	-2.59	0.01
PF-73	**6.489**	**-2.32**	**-0.24**				
PF-74	**6.578**	**-2.45**	**-0.09**				
PF-75	6.668	-1.54	0.18				
PF-76	6.757	-0.92	0.68				
PF-77	6.847	-1.24	0.40				
PF-78	6.936	-1.54	0.29				
PF-79	7.026	-1.78	0.58				
PF-80	7.115	-1.97	0.50				
PF-81	7.205	-2.41	0.13				
PF-82	7.294	-2.31	0.45				
PF-83	7.384	-2.42	0.49				
PF-84	7.473	-2.35	0.42				
PF-85	7.563	-2.08	0.53				
PF-86	7.652	-2.10	0.32				

[a] these data are not corrected for local $\delta^{13}C_{DIC}$ and $\delta^{18}O_{sw}$.

* Numbers in bold type: Medullar zone.

Tab.4. $\delta^{13}C$ and $\delta^{18}O$ mean values (± 1SD) of the four *C. rubrum* specimens. Isotope values were obtained from the annular and medullar zones. Values in parentheses represent the isotope range.

Sample	**Entire stem**		**Annular zone**		**Medullar zone**		**$\delta^{18}O_{eq}$ (‰ V-PDB)[a]**	**$\delta^{13}C_{eq}$ (‰ V-PDB)[b]**
	$\delta^{13}C$ (‰ V-PDB)	**$\delta^{18}O$ (‰ V-PDB)**	**$\delta^{13}C$ (‰ V-PDB)**	**$\delta^{18}O$ (‰ V-PDB)**	**$\delta^{13}C$ (‰ V-PDB)**	**$\delta^{18}O$ (‰ V-PDB)**		
RI (Branch)	-3.39 ± 0.47 (-4.40 to -2.62)	-0.54 ± 0.35 (-1.30 to 0.08)	-3.29 ± 0.50 (-4.22 to -2.62)	-0.42 ± 0.30 (-1.04 to 0.08)	-3.54 ± 0.41 (-4.4 to -2.96)	-0.72 ± 0.35 (-1.30 to -0.12)	0.98 ± 0.29	1.80
CO (Branch)	-4.53 ± 0.39 (-5.19 to -3.46)	-0.73 ± 0.22 (-1.10 to -0.22)	-4.44 ± 0.44 (-5.19 to -3.46)	-0.65 ± 0.20 (-0.97 to -0.22)	-4.71 ± 0.12 (-4.89 to -4.48)	-0.92 ± 0.13 (-1.10 to -0.71)	0.81 ± 0.21	1.90
MI (Base)	-1.93 ± 0.62 (-3.23 to -0.69)	-0.16 ± 0.32 (-1.02 to 0.43)	-1.94 ± 0.72 (-3.23 to -0.69)	-0.03 ± 0.26 (-0.61 to 0.43)	-1.91 ± 0.32 (-2.50 to -1.36)	-0.45 ± 0.27 (-1.02 to -0.08)	0.97 ± 0.21	2.20 ± 0.22
PF (Base)	-1.97 ± 0.84 (-6.35 to -0.27)	0.20 ± 0.61 (-2.70 to 0.89)	-1.61 ± 0.48 (-2.42 to -0.78)	0.43 ± 0.24 (-0.24 to 0.89)	-2.49 ± 0.97 (-6.35 to -0.27)	-0.14 ± 0.80 (-2.70 to 0.83)	1.44 ± 0.04	2.20 ± 0.22

[a] Values calculated using the equation by Bemis et al. (1998)

[b] Values calculated using the equation by Romanek et al. (1992)

Tab.5. Linear regression equations of $\delta^{18}O$ (Y) vs. $\delta^{13}C$ (X) obtained from the annular, medullar zones and the entire stem.

Sample	annular zone			medullar zone			Entire Stem			
	Equation	N	R^2	Equation	N	R^2	Equation	N	R^2	p-value
RI (Branch)	Y = 0.50 X+1.24	25	0.70	Y = 0.72 X+1.84	18	0.71	Y = 0.62 X+1.56	43	0.70	<0.0001
CO (Branch)	Y = 0.34 X+0.88	23	0.57	Y = 0.59 X+1.84	11	0.33	Y = 0.42 X+1.17	35	0.56	<0.0001
MI (Base)	Y = 0.26 X+0.48	49	0.52	Y = 0.55 X+0.61	21	0.44	Y = 0.28 X+0.38	71	0.28	0.000002
PF (Base)	Y = 0.29 X+0.90	51	0.36	Y = 0.69 X+1.57	35	0.69	Y = 0.60 X+1.38	86	0.68	<0.0001

Tab.6. Mean $\delta^{13}C$ and $\delta^{18}O$ values obtained from the two opposite sides of the annular zone.

Sample	**$\delta^{13}C$ (‰ V-PDB)**		**$\delta^{18}O$ (‰ V-PDB)**	
	Side 1	**Side 2**	**Side 1**	**Side 2**
RI (Branch)	-3.35 ± 0.50	-3.54 ± 0.53	-0.42 ± 0.20	-0.53 ± 0.46
CO (Branch)	-4.15 ± 0.33	-4.78 ± 0.29	-0.60 ± 0.22	-0.70 ± 0.16
MI (Base)	-1.49 ± 0.47	-2.66 ± 0.36	0.13 ± 0.17	-0.29 ± 0.15
PF (Base)	-1.89 ± 0.49	-2.09 ± 0.27	0.42 ± 0.16	0.17 ± 0.24

Tab.7. Least squares linear regression equations of $\delta^{18}O$ (Y) vs. $\delta^{13}C$ (X) calculated using values corrected for local $\delta^{18}O_{sw}$ and $\delta^{13}C_{DIC}$. The $\delta^{18}O_{intercept}$ values are calculated from the linear regressions at $\delta^{13}C$ = 0 ‰. For the calculations only the values from the annular zone were used.

	Sample	**Temperature (°C)**	**Equation**	**N**	**R^2**	**$\delta^{18}O_{intercept}$ (‰ V-PDB)**	**p-value**
Including the anomalous data point	RI (Branch)	16.37	Y = 0.50 X + 0.33	25	0.70	0.33	< 0.0001
	CO (Branch)	17.34	Y = 0.34 X - 0.15	24	0.57	-0.15	0.00002
	MI (Base)	16.45	Y = 0.26 X - 0.52	48	0.52	-0.52	< 0.0001
	PF (Base)	14.61	Y = 0.29 X - 0.14	51	0.36	-0.14	0.0001
Excluding the anomalous data point	RI (Branch)	16.37	Y = 0.37 X - 0.18	22	0.55	-0.18	< 0.0001
	CO (Branch)	17.34	Y = 0.33 X - 0.22	22	0.48	-0.22	0.0004
	MI (Base)	16.45	Y = 0.26 X - 0.52	48	0.52	-0.52	< 0.0001
	PF (Base)	14.61	Y = 0.29 X - 0.14	51	0.36	-0.14	< 0.0001